LUND UNIVERSITY

Degree Project in Sustainable Energy Engineering - MVKM05

Title: Solar Water Heating for Enhanced Electrolysis in Hydrogen Production

ALEXANDROS SARANTAKIS

Supervisor: Narmin Hushmandi
Examiner: Marcus Thern

June, 2026

Acknowledgements

I would like to express my sincere gratitude to **Solarus Renewables AB** and specifically to **Jan Cedervall**, for the opportunity and the joy he offered me to be engaged in such a fascinating and meaningful field. I would also like to thank **MG Sustainable Engineering AB**, especially **Joao Gomes**, **Ivan Acosta** and **Antonio Arto Delgado**, for providing valuable expertise and technical resources that were essential for the completion of my diploma thesis. Special thanks go to **Georgios Aspetakis**, a friend and PhD candidate at KTH Royal Institute of Technology, for his support through his technical knowledge during my effort to develop simulation models. I am also grateful to my Greek friends and colleagues in our master's program, **Panagiotis Pappas** and **Stefanos Naoumis**, for their support and their willingness to serve as the opposition during the presentation of my thesis. Finally, I would like to sincerely thank **Narmin Hushmandi** and **Henrik Davidsson** for accepting to be my supervisor and co-supervisor, as well as **Marcus Thern** for agreeing to serve as my examiner.

ISSN: 0282-1990

ISRN: LUTMDN/TMHP-26/5696-SE

Table of Contents

Abstract

As the need to limit the effect of climate change gets stronger, the transition to sustainable energy solutions becomes very important. Solar thermal energy and green hydrogen production represent two quite promising sustainable fields towards decarbonizing industrial processes and energy sectors. This thesis presents an extensive simulation and performance analysis of a solar thermal energy system designed to generate heated water for different kinds of electrolysis, destinated for hydrogen production, which can be combined with captured CO_2 and therefore production of electrofuels, such as methanol, whereas in the meantime this process reduces industrial emissions of CO_2 in the atmosphere.

The objective of this research is to evaluate technical and operational feasibility of implementing solar collectors for low-temperature electrolysis systems, applied on technical and meteorological data of the 8 MWp solar PV park of Vassiliko, Cyprus. Focusing on technologies applied on modern projects, dynamic simulation models were developed using a widely used simulation software, the Transient System Simulation Tool (TRNSYS). The models' performance was carried out under dynamic meteorological conditions; to the water flowrate needs and the water temperature configurations. Emphasis was placed, as well, on optimizing solar energy capture by simulating properly wind and infrared solar collectors (WISC) that are applied at the back of solar PV panels, as well as compound parabolic collectors (CPC) based on their technical data. The goal is the generation of 123.000 tons of heated water, at distinct operational temperature ranges, for the production of hydrogen that can contribute to a 10% decrease in the CO_2 emissions of a local cement industry, by combining them with hydrogen coming from electrolysis to produce methanol.

The simulation results of various configurations demonstrate that an integrated solar thermal system can effectively maintain required inlet fluid temperature ranges for Proton Exchange Membrane (PEM) and Anion Exchange Membrane (AEM) electrolysis methods. Solar water heating for AEM electrolysis proves to be a less demanding option since it can be processed only by applying collectors at a part of the present facilities of the solar PV park of Vassiliko, whereas the additional required facilities turn out to be less challenging. However, solar water heating for PEM electrolysis seems to be a more stable option in terms of thermodynamic utilization. It was discovered that a layout including two WISC (wind infrared sensitive collector) units in parallel connected in series with one CPC (concentrated power compound) unit presents quite good thermal efficiency and could be implemented at a significant part of the solar PV park, as well as in additional space close to it. By optimizing water mass flow rates and simulating various models, high thermal efficiency can be obtained, making the process thermodynamically viable. Ultimately, this work provides valuable insights and a robust modeling framework for designing the first stage of a sustainable and scalable energy system, whereas it highlights the significance of developing research on various other crucial parts of the project in order to make it highly efficient and environmentally sustainable. Nevertheless, as shown in the next chapters of the thesis, there are many kinds of studies that need to be done with the intention of turning a project like that into reality and evaluating all the impacting factors of an implementation like this.

Nomenclature

Latin letters

- A_G: Collector's gross surface area (m^2)
- Ar_C: Atomic mass of carbon (kg/kmol)
- Ar_H: Atomic mass of hydrogen (kg/kmol)
- Ar_O: Atomic mass of oxygen (kg/kmol)
- b_0: Incidence angle modifier parameter (dimensionless)
- c_p: Specific heat capacity of the working fluid under constant pressure (kJ/kg.K)
- E_L: Long-wave radiation from the sky (W/m^2)
- G: Total solar irradiance (W/m^2)
- G_b: Beam solar irradiance (W/m^2)
- G_d: Diffuse solar irradiance (W/m^2)
- $K_b(\theta)$: Incidence angle modifier for beam solar radiation (dimensionless)
- K_d: Incidence angle modifier for diffuse solar radiation (dimensionless)
- $\dot{m}_{fluid}$: water mass flow rate (kg/s or kg/hr)
- $\dot{Q}_{th}$: Thermal capacity / thermal load output (W)
- T_a: Ambient air temperature (K or °C)
- $T_{fluid,inlet}$: Inlet fluid temperature (K or °C)
- $T_{fluid,outlet}$: Outlet fluid temperature (K or °C)
- T_m: Mean fluid temperature (K or °C)
- u: Wind speed (m/s)
- $\dot{m}_{in,1}, \dot{m}_{in,2}$: water mass flowrates at the two inlets of the flow mixer (kg/s or kg/hr)
- $\dot{m}_{out}$: water mass flowrate at the outlet of the flow mixer (kg/s or kg/hr)
- $T_{in,1}, T_{in,2}$: water temperatures at the two inlets of the flow mixer (K or °C)
- T_{out}: water temperature at the outlet of the flow mixer (K or °C)

Greek letters

- α_1: Heat loss coefficient ($W/m^2.K$)
- α_2: Temperature dependence of heat loss coefficient ($W/m^2.K^2$)
- α_3: Wind speed dependence of heat loss coefficient ($J/m^3.K$)
- α_4: Sky temperature dependence of heat loss coefficient (dimensionless)
- α_5: Effective thermal capacity ($J/m^2.K$)
- α_6:Wind speed dependence of peak collector efficiency (m/s)
- α_7:Wind speed dependence of infrared radiation exchange (W/m^2K^4)
- α_8:Radiation loss coefficient (W/m^2K^4)
- α_{10}: Condensation/evaporative energy exchange dependence (J/kg)
- α_{11}: Rain dependence of thermal heat losses/gains (dimensionless)
- $\eta_{0,b}$: Optical thermal efficiency at normal incidence / beam (dimensionless)
- θ: Incidence angle of solar radiation (degrees or radians)
- σ: Stefan-Boltzmann constant (= $5{,}67 \times 10^{-8}$ $W/(m^2K^4)$)

Abbreviations

- AEM: Anion Exchange Membrane (Electrolysis method)
- CCS: Carbon Capture and Storage
- CPC: Compound Parabolic Concentrator
- CSP: Concentrated Solar Power
- EU: European Union
- IEA: International Energy Agency
- FPC: Flat-Plate Collector
- GHG: Greenhouse Gas
- IAM: Incidence Angle Modifier
- MWp: Mega-Watt peak (meaning the maximum power that the solar PV park can produce)
- PEM: Proton Exchange Membrane (Electrolysis method)
- PID: Proportional-Integral-Derivative (Automatic Control system)
- PV: Photovoltaic
- PVT: PhotovoltaicThermal
- RES: Renewable Energy Sources
- TRNSYS: Transient System Simulation Tool (the software used for the simulations made)
- WISC: Wind and Infrared Sensitive Collector
- $\Delta H_{C,298K}$: energy required for the completion of a chemical reaction at temperature of 298K.

1. Introduction

1.1. Background and context

As concerns of climate change emerge, the world is in search of alternative and renewable forms of energy aiming to decrease the impact of climate change, limit its consequences in the next decades and face depletions of fossil fuels. Conventional energy production forms (coal, oil and natural gas) are the largest source of greenhouse gas (GHG) emissions worldwide, supplying roughly 84,5% of global primary energy and generating about 66% of the global electricity (Saldaña et al., 2025). As a result, fossil fuel–based power plants release large amounts of harmful pollutants into the atmosphere, including carbon dioxide (CO_2), nitrogen oxides (NO_2) and sulfur dioxide (SO_2). The increase of GHG emissions -around the globe- is mainly driven by the increased use of coal, oil and natural gas to satisfy rapidly rising energy demands. In this context, solar energy offers a promising solution to energy poverty. By replacing conventional fossil fuels for heat and electricity production, solar power can significantly reduce GHG emissions as well as air pollution, while expanding access to clean and reliable energy (Izam et al., 2022).

Global efforts towards the expansion of clean energy have led to renewables supplying approximately 24% of the world's annual electricity, and this share continues to rise each year (Saldaña et al., 2025). Among renewable sources, solar energy has attracted significant global attention because of its strong potential to help address the energy crisis and combat global warming. Photovoltaic (PV) technology, which converts sunlight directly into electricity, plays a significant role in decreasing GHG emissions by reducing reliance on fossil fuels for power generation. Regarding the renewable energy sector, solar PV accounts for about 24% of renewable-based electricity production, highlighting their growing contribution to the global energy supply. In recent years, solar PV has become one of the fastest-growing renewable energy technologies, expanding at a higher annual rate than other sources such as hydrogen, wind or bioenergy. Improvements in technology and falling production costs have made solar electricity cost-competitive compared to conventional forms of power generation, as well (Liu et al., 2024). In 2021 alone, global solar power generation rose by approximately 179 TWh (an increase of about 22%) bringing total photovoltaic electricity annual production to over 1000 TWh (Balliff et al, 2022).

One of the main challenges faced by photovoltaic (PV) technology is thermal management, since a reduction in maximum power output can be caused by an increase in ambient temperature. As shown in Fig.1.1, although a rise in temperature does not significantly reduce the PV panel current (it may even increase slightly), it leads to a noticeable decrease in the output voltage. This voltage drop results in lower overall power production and reduces the efficiency of the PV cells (Al-Ghezi et al., 2022). Consequently, the solar PV cooling becomes in many cases considerably necessary. A cooling system performance is always impacted by a combination of technical, environmental and operational factors that interact with each other. Ambient temperature and solar irradiance affect significantly the thermal load of the system, as higher environmental temperatures and stronger solar radiation increase surface and internal temperatures. The overall design efficiency of a heat release system determines how effectively excess heat can be removed. Proper thermal regulation is essential to maintain performance and extend system lifespan (Ahmed et al., 2024).

Material selection and structural design are also very important concerning cooling effectiveness, because choosing materials with high thermal conductivity and strong resistance to corrosion enhances heat transfer and system resilience. The accumulation of dust on surfaces reduces the heat transfer capability and may obstruct ventilation pathways. Dust particles can influence notably the intensity of the impact, since these particles can often penetrate deeper into system components. Regular cleaning and preventive maintenance are therefore necessary to sustain optimal cooling performance and prevent overheating. Moreover, environmental conditions can further affect cooling systems. Humidity can promote corrosion and material degradation, while wind may either assist or disrupt airflow patterns. Rain introduces moisture-related risks, whereas salt exposure, especially in coastal regions, accelerates corrosion processes (Ahmed et al., 2024).

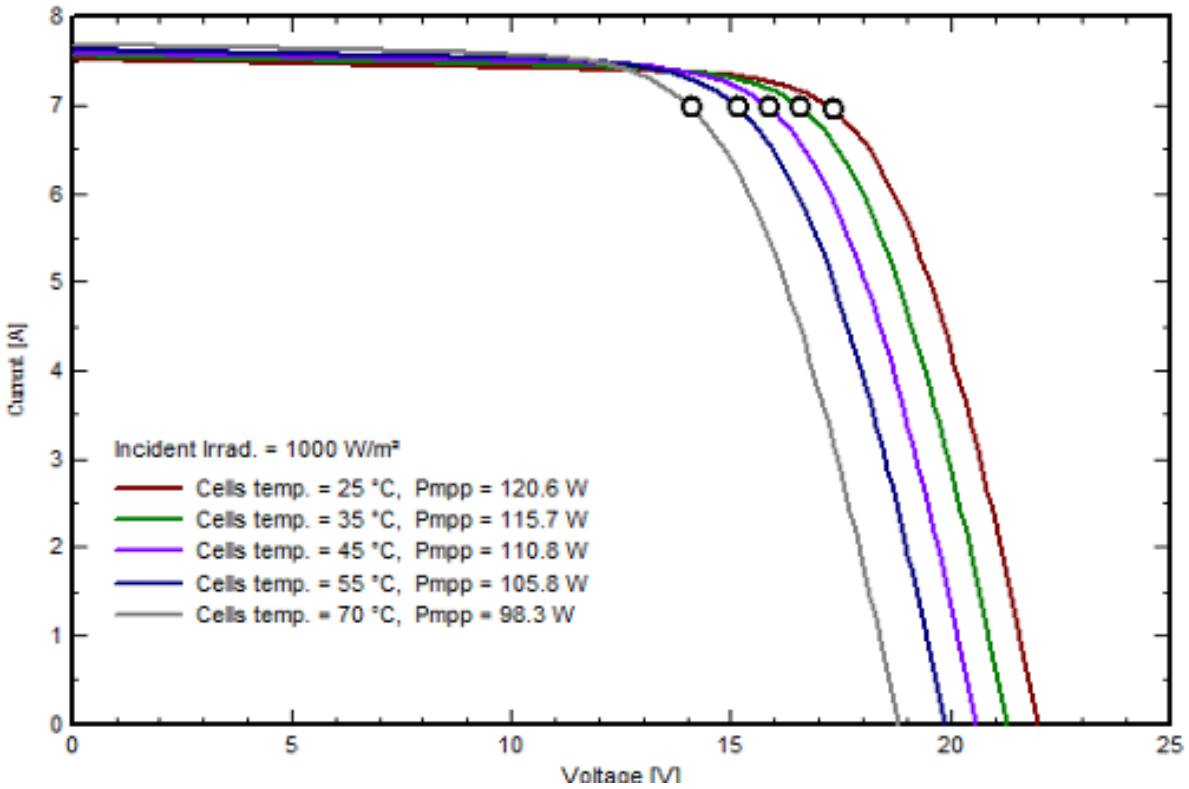

Fig. 1.1: The I-V curves of a PV panel, installed in Iraq, at constant solar irradiance (1000W/m^2) and different PV cells' temperature levels on it. The small white dots indicate the points of maximum power of the PV panel (which is the product of current and voltage, P=I×V). As can be seen, at higher temperatures, the maximum power of the panel decreases. Source: Al-Ghezi et al., 2022

To capture more of the solar energy available, hybrid photovoltaic-thermal (PVT) configurations have been developed, to produce both electrical and thermal energy at the same time. PVT models combine concentrating collectors of solar thermal energy with PV cells in the same modules. An example of a configuration of this kind is a system that combines PV modules with collectors that have collection pipes or troughs and are installed on the rear side of the panel, often called WISC (Wind and Infrared Sensitive Collectors) (Mehnert et al., 2017). Water serves as the working fluid and circulates through the parallel pipes or troughs with the help of a DC pump, which can be powered either by the PV module itself or by an external energy source. When the

system is exposed to solar radiation, the excess heat generated by the PV module is absorbed and transferred to the circulating water. The heated water is then directed to an insulated water storage tank, where it can be used for other thermal applications (Siecker et al., 2017).

Another example of a PVT system, combining conversion of solar energy to both electricity and thermal energy are the solar compound parabolic concentrators (CPC). The primary application of CPC technology is in solar energy systems, such as PV, solar thermal and hybrid PVT configurations. Researchers of PVT systems -around the world- highlight the significance of CPC technology as a leading one regarding stationary solar energy concentration devices. In its most basic configuration, a CPC consists of two symmetric parabolic reflecting segments designed to redirect incident solar radiation from the entrance aperture toward a receiver at the exit aperture. The left and right reflecting surfaces are derived from two distinct parabolas, with the receiver positioned between their respective focal points. The axes of these parabolic segments are tilted away from the central axis of the CPC by a specific angle, defined as the acceptance half-angle. Any solar radiation entering the aperture within this angular range is funneled to the receiver, either through direct incidence or via multiple reflections. Consequently, the primary design parameters for an ideal CPC are the determination of the acceptance half-angle and the dimensions of the flat receiver (Masood et al., 2022).

Fig. 1.2: Typical example of a WISC, designed to abstract thermal energy from a PV panel. Source: Mehnert et al., 2017.

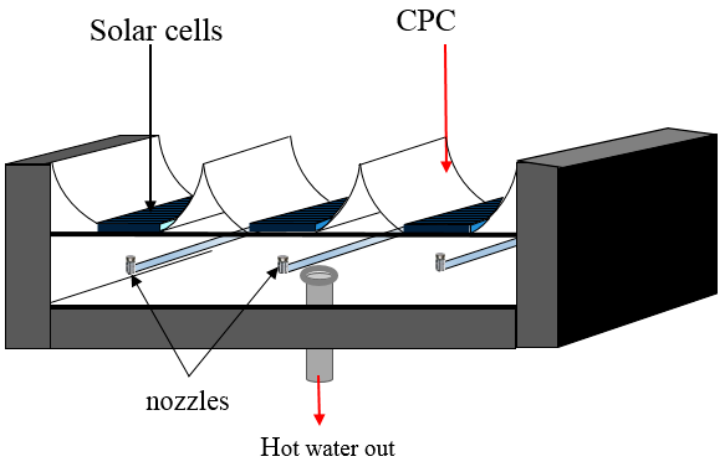

Fig. 1.3: Typical example of hybrid CPC-PVT system, designed to produce both electricity and thermal energy. Source: Jaaz et al., 2017

While existing literature thoroughly covers solar PV cooling methods across various projects, a distinct research gap remains regarding the integration of wind and infrared sensitive collectors (WISC) combined with compound parabolic concentrators (CPC) for heating water designated for low-temperature industrial applications.

Conventionally, the primary objective of applying solar WISC collectors is the optimization of a PV panel's electrical efficiency; in contrast, this study does not focus on thermally electrical optimization. Instead, it evaluates the precise volumetric and fluid dynamic water requirements within a collectors' layout to achieve specific temperature thresholds required for different methods of electrolysis. Specifically, utilizing recovered thermal energy from an existing utility-scale PV park to drive low temperature electrolysis methods (such as AEM, PEM and alkaline systems) has not yet been dynamically modeled, especially under highly localized, semi-arid meteorological conditions like those of Cyprus. Consequently, identifying direct comparative baseline data in existing literature is not feasible due to lack of documented applications sharing identical or similar configurations, thermal goals and climatic boundaries. To overcome this limitation and address the established gap, this thesis develops an independent, transient thermo-hydraulic framework using TRNSYS simulation software to establish a baseline performance standard for such integrated systems.

1.2. Statement of the thesis project

In the region of Vassiliko in the southern part of Cyprus, an 8 MWp solar PV park, shown in Figure 1.4 below, has been in operation since 2020, covering a geographical area of approximately 30 hectares. The park is owned by Vassiliko Cement Works Public Company Ltd. And it was constructed at a cost of €6,5 million and, according to the company, covers approximately 10% of the electricity needs of the company's facilities. Moreover, the operation of the photovoltaic park contributes to the reduction of approximately 100.000 tons of CO_2 per year (Vassiliko Cement Works Public Company Ltd., 2020).

Fig. 1.4: The solar PV installation in Vassiliko, Cyprus. Source: Google Maps

Fig. 1.5: Location (with red dot) of the solar PV installation in the island of Cyprus. Source: Google Maps

According to the Cyprus Energy Regulatory Authority (2019), the project for the construction and operation of the PV park at Vassiliko was implemented by the Ministry of Energy, Commerce and Industry (MECI) of Cyprus in an effort to reduce the dependency on fossil fuels in the Republic of Cyprus, as well as to mitigate greenhouse gas emissions, in alignment with the United Nations' 17 Sustainable Development Goals. As mentioned by Eurostat (2025), the Republic of Cyprus is heavily dependent on fossil fuels for its energy needs. In 2023, renewable energy sources (RES) accounted for only 11,1% of the country's total energy mix. Fossil fuels were responsible for 79,5% of electricity production, while oil products account for 55,9% of total final energy consumption. In contrast, the direct use of RES represented 13,5% of total final energy consumption. Electricity prices in the Republic of Cyprus during the first semester of 2024 were among the highest in the European Union (EU). Household electricity prices reached €0,324/kWh, the sixth highest in the EU, compared to the EU average of €0,292/kWh. For non-household consumers, electricity prices were even higher compared to the rest of the EU, reaching €0,245/kWh, the second highest in the Union, while the EU average stood at €0,189/kWh.

Furthermore, the country exhibits a very high level of energy import dependency. In 2023, the dependency rate reached 96,1% in the first semester and 92,2% in the second semester, significantly exceeding the EU averages of 56,9% and 58,3%, respectively. As mentioned by the International Energy Agency (IEA, 2026), in 2023, electricity and heat production is responsible for 50,3% of the CO_2 emissions (and its equivalents GHG) in the country and transport for 32,5%. Transport is the major sector of the final total energy consumption, having a share of 42,3% of it. Studying the data above makes it obvious that projects like the 8 MWp solar park in Vassiliko are considered necessary for the transition of the country to cleaner energy solutions, greater dependency of the country on its own energy resources and lower energy costs. Additionally, the utilization of other types of fuels, becomes likewise necessary since the sector of transport is the most energy-consuming and the energy production sector is the most polluting one in the Republic of Cyprus, leaving at the second place the transport sector. In this spirit, the production of electrofuels (e-fuels) stands as an alternative potential option that could replace a portion of the present need for conventional fuels and decrease the need for imported fuels on the island.

The term e-fuel is used to define the production process of liquid or gaseous fuel that stores electricity via electrolysis and the carbon source into valuable fuel products that are used as a storage buffer for electricity produced by renewable energy sources (Ridjan, 2015). The easiest way to make e-fuel is to produce hydrogen through electrolysis. This hydrogen can then be used directly to power fuel. However, hydrogen can also be taken and inserted into more advanced chemical processes. This creates liquid fuels (like synthetic gasoline or diesel) that are chemically identical to the conventional ones used today. Hydrogen combined with carbon dioxide (CO_2) can produce methane and methanol, while combining it with carbon monoxide (CO) can yield products such as methane or propane (Malins, 2017). E-fuels are considered a promising option for multiple transport sectors, such as aviation, shipping or road transport, because many of them are compatible with the current vehicle fleet and can be distributed through existing fuel infrastructure with limited additional investment. Furthermore, e-fuels can support the integration of renewable energy sources by utilizing surplus electricity generated during periods of high production or low demand. The production process may also create useful by-products, including high-purity oxygen and heat, which can have commercial value (Grahn et al., 2022).

Methane production with the use of carbon dioxide: $CO_2 + 4H_2 \rightarrow CH_4 + 2H_2O$, $\Delta H_{C,298K}$=-164,7 KJ/mol (Huang et al., 2024) [eq.1]

Methanol production with the use of carbon dioxide: $CO_2 + 3H_2 \rightarrow CH_3OH + H_2O$, $\Delta H_{C,298K}$=-49,16 KJ/mol (Kiss et al., 2016) [eq.2]

Organic fuel production with the use of carbon monoxide: $nCO + (2n+1)H_2 \rightarrow C_nH_{2n+2} + nH_2O$ [eq.3]

Towards that direction, organic compounds that exist in pollutant industrial waste can be utilized to produce e-fuels when combined with hydrogen, as shown at the chemical equations above. For this reason, among many, the carbon capture and storage (CCS) technology is a scientific and technical field that can be utilized, in the future, for the energy needs of many parts of the world and among them the island of Cyprus. Modern CCS technology brings decades of technical experience in 'sweetening' natural gas, a process used since the 1930s to remove excess CO_2 from fuels using amine-based scrubbing.

While this method was originally designed to purify gas for commercial sale, it is now being adapted to pull carbon directly from industrial exhaust. Similarly, the oil industry's long-standing practice involves transporting and pumping CO_2 underground to help extract more oil and provides the blueprint for carbon capture and storage (CCS). By utilizing these same injection techniques, CO_2 can be permanently stored in deep geological formations (Smit, 2016). Consequently, a carbon capture system at a facility such as the Vassiliko Cement Works Public Company Ltd. could be effectively integrated with the company's solar park to produce e-fuels. In this scenario, the implementation of solar thermal and hybrid PV-thermal (PVT) systems would provide critical industrial heat. This thermal energy enhances water electrolysis efficiency, thereby optimizing the production of hydrogen. This hydrogen can then be utilized as a standalone e-fuel or synthesized with carbon compounds to create various other electrofuels.

Methanol can be regarded as a pivotal e-fuel in the shift from fossil fuels to renewable energy because of its versatility and high performance. With an octane rating of 113 (significantly higher than standard fuels) and a density roughly half that of gasoline, it offers important combustion characteristics. Blended with traditional gasoline for use in standard vehicles can offer a wide range of transport applications without needing engine upgrades. A common high-concentration blend is M85, consisting of 85% methanol and 15% gasoline. Methanol serves as a stable, liquid medium for the efficient storage and long-distance transport of hydrogen, whereas it is used, as well, to manufacture polymers, synthetic hydrocarbons, and even single-cell proteins. Essentially, its ease of transport and compatibility with existing infrastructure make it a practical bridge toward a sustainable energy future (Dalena et al., 2018).

Regarding the part of electrolysis and hydrogen production, temperature is a primary factor impacting the electrical demand of an electrolysis cell, as the process becomes significantly more efficient at higher temperatures. From a thermodynamic perspective, this occurs because the energy potential required to split a water molecule decreases as temperature rises. Additionally, higher temperatures boost both the ionic conductivity and the rate of surface reactions within the electrolyte. Thus, high-temperature electrolysis requires less total energy to achieve the same current density as low-temperature methods (Mazloomi et al., 2012). To achieve higher temperatures, solar thermal technologies can be utilized, such as Concentrated Solar Power (CSP)

collectors or hybrid PV-thermal (PVT) systems, which capture and repurpose solar heat (Zhang et al., 2013).

There are mainly three types of electrolysis:

- Proton Exchange Membrane (PEM)
- Alkaline
- Anion Exchange Membrane (AEM)

The conventional commercialized PEM electrolysis, also known as low temperature one (LT-PEME) has an operation temperature range usually at 50º-90ºC. However, in recent years, there has been development regarding high temperature PEM electrolysis (HT-PEME) which has an operation temperature range above 100ºC. A mature electrolysis technology is the alkaline type, too, which functions between 70º and 90º C. The AEM type of electrolysis is an emerging technology that seems quite promising and presents a function range of 40º-60ºC. However, it is still at a research and development (R&D) level and so far, it is not considered mature technology ready to be commercialized (Kumar & Lim, 2022), (Corti, 2022).

2. Methodology and thesis objectives

Based on the operational data from Vassiliko Cement Works Public Company Ltd., an integrated e-fuel production system could be developed using a multi-stage heating approach. First, a PV cooling system utilizing retrofitted thermal collectors installed on the back of the solar panels would preheat the water supply. This water would then be directed into Concentrated Solar Power (CSP) collectors to reach higher temperatures. Finally, the heated water would be fed into an electrolysis chamber. The resulting hydrogen could then be combined with carbon compounds captured from the cement industry's exhaust to produce e-fuels. In this thesis, there is an investigation regarding the specific quantity of water required for heating and subsequent electrolysis to produce hydrogen which serves as a precursor for methanol production. Methanol holds significant potential for transportation applications; notably, its synthesis requires lower quantities of hydrogen—and consequently less water—compared to other e-fuels, such as methane (Dalena et al., 2018).

The theoretical objective of this study is to evaluate how water can be heated at appropriate temperature ranges for different kinds of electrolysis, to produce enough hydrogen to react with organic compounds and thus achieve a 10% reduction in the factory's industrial CO_2 emissions, corresponding to a target of 100.000 tons of CO_2. Setting a goal of 10% is not certain, in advance, since a regional planning study must be implemented, too, in order to evaluate if the additional facilities required to achieve this target can be realistically constructed in the greater region of the solar PV park. However, finding out the necessities of this target can give a greater picture that can be quite useful for future studies of the project, at least partially if not completely. At the next stage, it will be determined how many collectors, and of which kind, can be applied in order to heat the required quantities of water. This study evaluates the integration of solar thermal retrofit collectors into a part of the existing PV installation and at a second stage the implementation of solar CSP collectors.

The purpose of the WISC collectors is to absorb excess heat from the PV panels, something that can increase their electrical efficiency. The WISC collectors transfer the recovered heat to water flowing through a network of pipes. The heated water is then driven throughout PV installations using pumps. However, this study does not deal with the optimization of the solar park's PV panels cooling. Such an approach would require a massive facility and huge amounts of water even to cool only a part of it. Instead, the main goal of the WISC collectors applied on the back of the PV panels will be to heat large amounts of water to high temperatures as much as possible. This application may have a positive impact on the electrical efficiency of the PV panels due to a decrease in the panels' temperature, but this is not the main objective of the study. In this work, it will be evaluated how efficiently the water can be heated in the first stage in order to be directed afterwards to another heating stage.

In this way, a solar PVT system can be applied more efficiently and at lower cost, allowing the utilization of CSP collectors in a subsequent stage to be better implemented for the electrolysis of water in a next stage and the production of hydrogen as an e-fuel itself or hydrogen that is necessary for the production of other organic e-fuels. The implementation of CSP collectors can enhance even more the heated water temperature making it suitable for various types of electrolysis. Consequently, it must be determined how many PV collectors from the Vassiliko solar PV park should be utilized and how many concentrated solar collectors are required to achieve the 10% CO_2 reduction target. The objective is to optimize the heated water mass flow rates and

maintain the appropriate temperature ranges to ensure the system operates at a high efficiency.

The V1 PVT-SP collector is the WISC technology selected for this project. Originally developed as a polymer-based heat recovery medium for heating, ventilation and air-conditioning (HVAC) applications, the V1 PVT-SP has been repurposed as a flat-plate collector (FPC) retrofit solution for PV panels. Its design has been optimized to enhance thermal performance for low-grade heat applications, operating at temperatures up to 60°C. The specific collector has been developed by SolarPeak. The V1 PVT-MG is a PVT compound parabolic collector (CPC), developed by Double MaReCo, that combines photovoltaic and thermal technologies to increase overall energy efficiency. It operates as a low-concentration solar collector with a symmetric CPC reflector design. The system can capture solar radiation throughout the day without the need for tracking, something that allows fixed installation. The absorber incorporates solar cells embedded in silicone gel, which can minimize thermal stress on the PV modules. This collector is intended for low-medium temperature industrial applications, with an operating temperature reaching up to 140°C (Dannemand et al., 2025).

Based on the data of the solar park at Vassiliko, Cyprus, there will be needed a modification of the V1 PVT-SP collector's dimensions, to be adapted to the park's panels' dimensions in real life future applications. The goal of this thesis is to optimize the layout of the heating water system by simulating different feasible configurations using the solar technology software TRNSYS. By incorporating local solar radiation data from Vassiliko, Cyprus; the simulations can evaluate the system's efficiency for the specific installation site and assess how its implementation can enhance electricity production. TRNSYS is used in various solar thermal studies for similar applications and can provide reliable and valuable solutions. Thus, by simulating different configurations of V1 PVT-SP and V1 PVT-MG collectors, this study will evaluate whether a system like that can serve as a viable solution and determine an efficient layout through the optimization of connecting and adjusting flow rates and collectors by using various relevant equations.

Fig. 2.1: The V1 PVT-SP solar thermal retrofit collector, developed by SolarPeak. Source: Dannemand et al., 2025.

Fig. 2.2: The V1 PVT-MG solar thermal retrofit collector, developed by Double MaReCo. Source: Dannemand et al., 2025.

Table 2.1: The V1 PVT-SP solar thermal retrofit collector technical characteristics. Source: Dannemand et al., 2025.

Parameter / Specification	Value
Temperature levels, °C	5 - 60
Absorber material	ABS
Applications	Heat pump integration, pool heating
Gross area, m²	0,910
Dimensions, mm	1655 x 550
Optical thermal efficiency, $\eta_{o,b}$ (beam)	0,535
Incidence angle modifier for diffuse solar radiation, Kd	0,93
Heat loss coefficient, α_1 [W/m²K]	13,47
Temperature dependence of heat loss coefficient, α_2 [W/m²K2]	Not significant
Wind speed dependence of heat loss coefficient, α_3 [J/m³K]	8,465
Sky temperature dependence of heat loss coefficient, α_4	0,84
Effective thermal capacity, α_5 [J/m² K]	18.890
Wind speed dependence of peak collector efficiency, α_6 [m/s]	0,109
Wind speed dependence of infrared radiation exchange, α_7 [W/m²K⁴]	Not significant
Condensation/evaporation dependence, α_{10} [J/kg]	-1021,00
Rain dependence of thermal heat losses/gains, α_{11}	0,41

Table 2.2: The V1 PVT-MG parabolic solar concentrating collector technical characteristics. Source: Dannemand et al., 2025.

Parameter / Specification	Value
Collector type	CPC-PVT
Temperature levels, °C	20 -140
Absorber material	Aluminum 6063
Application	District and Industrial Heating
Gross area, m²	2,57
Optical thermal efficiency, $\eta_{0,b}$ (beam)	0,49
Incidence angle modifier for diffuse solar radiation, Kd	0,86
Heat loss coefficient, a1 [W/m²K]	3,34
Temperature dependence of heat loss coefficient, a2 [W/m²K²]	0,013
Coefficient for electrical efficiency [-]	0,008
Coefficient for electrical efficiency – thermal dependency [1/K]	-0,0003

The coefficients shown at the tables above refer to the flexible quasi-dynamic model that is used as the foundation for modeling the thermal performance of both WISC and CPC-PVT collectors and are shown in the equation below (ISO, 2017). This model considers how factors such as direct and diffuse solar radiation, the temperature of the working fluid, wind speed, the angle at which sunlight strikes the collector and the system's thermal capacity affect performance. The performance coefficients are determined using multi-linear regression based on measurements taken from outdoor testing of the collector (Lämmle et al., 2017), (Kramer et al., 2023).

In the context of solar energy engineering and research, the guidelines followed are provided by the International Organization for Standardization (ISO) and serve as mathematical and experimental baselines for defining how solar collectors of different kinds interact with their environment. The specific baselines constitute the ISO 9806:2017 standard, which is globally recognized as a set of testing methods established by ISO for evaluating the fluid heating performance, durability, and reliability of solar thermal collectors. According to ISO9806:2017, the equations related to the thermal loads are:

$$\dot{Q}_{th} = A_G[n_{0,b}(K_b(\theta)G_b + K_d G_d) - a_1(T_m - T_a) - a_2(T_m - T_a)^2 - a_3 u(T_m - T_a) + a_4\left(E_L - \sigma {T_a}^4\right) - a_5\frac{dT_m}{dt} - a_6 uG - a_7 u\left(E_L - \sigma {T_a}^4\right) - a_8(T_m - T_a)^4] \text{ (W)} \quad \text{[eq.4]}$$

$$\dot{Q}_{th} = \dot{m}_{fluid} c_{p,fluid}\left(T_{fluid,out} - T_{fluid,in}\right) \text{ (W)} \quad \text{[eq.5]}$$

$$T_m = \frac{T_{fluid,in} + T_{fluid,out}}{2} \ (K) \quad \text{[eq.6]}$$

where A_G: collector's surface (m^2) T_m: mean fluid temperature (K). T_a: ambient air temperature (K), G_b & G_d: Beam and Diffuse solar irradiance (W/m^2). G: total solar irradiance ($G = G_b + G_d$). u: Wind speed (m/s), E_L: Long-wave radiation from the sky (W/m^2). σ: Stefan-Boltzmann constant ($\sigma = 5{,}67 \times 10^{-8}$ $W/(m^2K^4)$). $K_b(\theta)$: incidence angle modifier for beam solar radiation (dependent on the incidence angle), K_d: incidence angle modifier for diffuse solar radiation, $\dot{m}_{fluid}$: fluid flowrate (kg/s, but

in the simulation models developed, it is defined in kg/hr), θ: incidence angle (rads or degrees for the simulation models). It is widely used as a generic equation, as shown below, regarding the incidence angle modifier, often mentioned with its initials (IAM).

$$K_b(\theta) = 1 - b_0(\frac{1}{cos\theta} - 1) \quad \text{[eq.7]}$$

where the parameter b_0 is chosen to suit the kind of collector under consideration, the geometry and the values of the solar angles (Strobach et al., 2013).

The terms representing rainfall and surface moisture have been omitted from the collector model due to the local meteorological conditions in Cyprus (Neophytides et al., 2024). Because the system's peak performance occurs during long, dry periods, the thermal impact of rain is statistically insignificant. Similarly, the energy exchange from condensation is treated as a minor factor that does not materially alter the overall efficiency results for this unglazed PVT application. Also, there is not any reference regarding the radiation loss coefficient at the technical data of the V1 PVT-SP collector, so this coefficient is considered zero for this case, whereas wind speed dependence of infrared radiation exchange is considered not significant, according to the same data. Thus, based on Table 1, the equation [1] for the V1 PVT-SP and the V1 PVT-MG collectors becomes:

$$\dot{Q}_{th,V1\ PVT-SP} = 1{,}95[0{,}535(K_b(\theta)G_b + 0{,}93G_d) - 13{,}47(T_m - T_a) - 8{,}645u(T_m - T_a) + 0{,}84\left(E_L - 5{,}67 \times 10^{-8}{T_a}^4\right) - 18890\frac{dT_m}{dt} - 0{,}109uG] \text{ (W)} \quad \text{[eq.8]}$$

and

$$\dot{Q}_{th,V1\ PVT-MG} = 2{,}57[0{,}49(K_b(\theta)G_b + 0{,}86G_d) - 3{,}34(T_m - T_a) - 0{,}013(T_m - T_a)^2 \text{(W)} \quad \text{[eq.9]}$$

By using TRNSYS, it can be evaluated on how many collectors can certain quantities of water pass through, in order to be heated to a temperature range suitable for different types of electrolysis. Layouts are developed in order to determine which one performs best in each case and in the end which of them may be considered the optimal choice. It should be noted that Cyprus, as an island, has a semi-arid climate, and many areas of the island experience water shortage problems, increased in the last few years, mainly due to the climate change and its impact on the region (Neophytides et al., 2024). Therefore, for a project like this, it must be assessed, in the future, whether the existing desalination facilities are adequate or whether additional facilities of this kind need to be constructed.

Two models were developed in TRNSYS to simulate distinct cases: the first utilizes only the V1 PVT-SP collector, while the second incorporates both the V1 PVT-SP and V1 PVT-MG collectors. On the second case, it is evaluated not only the thermodynamic performance of a V1 PVT-SP collector connected in series with a V PVT-MG collector, but the performance of many V1 PVT-SP collectors in parallel connected in series with a V1 PVT-MG collector. The option of connecting various V1 PVT-SP in series was not chosen, since this could create greater ranges between minimum and maximum flowrates and consequently make the application of variable speed pumps a harder problem to solve. Moreover, the parallel connection of V1 PVT-SP collectors can yield higher thermal efficiency. For the scope of this study, the tank and pipes thermal loss coefficients are assumed to be negligible. The PID controllers and tank thermal

coefficients may be analyzed in greater detail in future research. Optimizing all system parameters simultaneously is a complex task that typically requires significant working hours and a collaborative team of engineers to account for regional, financial and material limitations.

The scientific questions coming to the surface are the following:

- What is the number of each type of collectors that must be chosen to generate heated water at quantities that can ensure efficient hydrogen production for the later production of methanol with the utilization of 100.000 tons of CO_2.
- How the water mass flowrates must be adjusted to ensure water heating at the required operational temperature ranges of each electrolysis method.
- Which configuration layout presents the best thermodynamic efficiency.

Beyond the primary scientific questions, several operational parameters required careful configuration, such as the storage tank fluid thresholds and system operational metrics. Since optimizing single variable simultaneously falls outside the scope of this thesis, a dedicated effort was made to establish feasible and realistic boundary constraints. Specifically, appropriate minimum and maximum tank levels were defined to ensure stable closed-loop hydraulics, while practical pump scheduling hours and PID control configurations were implemented to preserve the stability of the layouts' systems. Objective of this project, along with the optimal utilization of thermal loads produced, is the proper utilization of the available water resources. For example, it would be highly inefficient and unsustainable to allow water that has not yet reached the target temperature to be discarded; instead, such resources are recirculated and stored in reservoirs to preserve and reduce the waste of water. Guided by this principle, the various configurations were developed in the next chapter. Regarding water properties, for the simulation models the specific heat capacity (c_p) was chosen to be 4,19 KJ/kg.K which is an average value used under constant pressure and at temperatures below 100ºC. Water density was chosen to be 1000 kg/m^3 as a typical density value of water.

Table 2.3: Table containing necessary technical data of the 8 MWp PV solar park at the region of Amalas in Vassiliko, Cyprus, as well as the annual emissions of the Vassiliko Cement Works factory.

Solar PV park in Vassiliko, Cyprus	**Data**
Collectors' slope	25º
Collector's dimensions	1,995m x 0,992m
Number of PV collectors	approx. 23.000
Vassiliko Cement Works annual emissions	**Data**
CO_2 emissions	approx. 1.000.000 tons/year
CO emissions	a few hundred tons/year

As the data of Table 2.3 indicates, the V1 PVT-SP collector cannot be directly attached to the PV panels in this specific solar park because its dimensions are significantly smaller. In a practical application, this type of collector would require a modification of its dimensions to match the existing panels. Consequently, for the purpose of this project, it is assumed that the integrated collectors have the same surface area as the PV panels, which is equal with 1,95m^2.

2.1. Single collector model

In the single collector model, a closed-loop system is created and simulated. Water is heated as it passes through the V1 PVT-SP collector and is subsequently directed to a thermostatic 3-way valve (how this valve works is elaborated in Chapter 3). If the water temperature is equal or above the required setpoint, it is discharged from the loop. Otherwise, it is recirculated into the loop via a flow mixer and stored in a tank. This tank features a high/low-level control system that signals a pump to supply fresh water through the flow mixer when necessary. Additionally, the pump supplying the collector is controlled by an equation-based timer, restricting operation to daylight hours. The collector model has a PID control system integrated to maintain the water outlet temperature as close as it gets to the setpoint temperature of 57,5ºC.

2.2. Two collectors' model

In the second model, once again a closed-loop system is created and simulated. Water is first heated by one or several V1 PVT-SP collectors connected in parallel and directed into a V1 PVT-MG collector which is connected in series. A thermostatic 3-way valve at the exit of the second collector determines the flow path, based on the water temperature. If the temperature is sufficient, the water exits the loop; if not, it recirculates through the flow mixer back into the tank. This tank features a high/low-level control system that signals a pump to supply fresh water through the flow mixer when necessary. As in the previous model, the primary pump for the V1 PVT-SP collector operates via an equation block timer synchronized with daylight hours. The PID control system of the V1 PVT-SP collector remains active at a temperature setpoint of 57,5ºC whereas the V1 PVT-MG collector's one stays inactive.

2.3. Stoichiometry and water electrolysis calculations

According to Table 2.3, a 10% reduction in CO_2 emissions is equivalent to approximately 100.000 tons of CO_2 per year. Consequently, the production of methanol (as an e-fuel) would require great quantities of electrolyzed water, from which there is hydrogen production necessary for the chemical formation of methanol, as shown at the chemical formulas below.

Water Electrolysis: $2H_2O \rightarrow 2H_2 + O_2$

Methanol production: $CO_2 + 3H_2 \rightarrow CH_3OH + H_2O$

Atomic masses of carbon, hydrogen and oxygen: Ar_C=12,0096 kg/kmol; Ar_H=1,008 kg/kmol; Ar_O=15,999 kg/kmol

According to the stoichiometry of the chemical equation for the formation of methanol, one kmol of CO_2 requires 3 kmols of H_2. One kmol of CO_2 weighs 12,0096 + (15,999x2) = 44,0094 kg, while 3 kmols of H_2 weigh 3x(2x1,008) = 6,048 kg. Therefore, 1 kg of CO_2 requires 6,048/44,0094 = 0,13743 kg of H_2.

Similarly, 1 kmol of H_2O electrolyzed yields 1 kmol of H_2. Since 1 kmol of H_2O weighs (2x1,008) +15,999 = 18,015 kg and 1 kmol of H_2 weighs 2,016 kg, 1 kg of H_2 is derived from 8,936 kg of H_2O. To process this amount, the synthesis would necessitate the electrolysis of $100x10^6$x0,13743x8,936 = 122.807.448 kg of H_2O.

Thus, by aiming to utilize the quantities of CO_2 produced and turn it into methanol, the required amount of heated water is approximately 123.000 tons per year.

3. Developing models in TRNSYS

The weather data used in the TRNSYS simulation were obtained from the meteorological station at Larnaca International Airport in Cyprus, located approximately 24 km (in a straight line) from the Vassiliko solar PV park.

Table 3.1: Table containing all the components used in TRNSYS models simulations with their application and their type name in the software environment.

Components	**Type**
Weather File	Type15
V1 PVT-SP collector	Type1286_v2a
V1 PVT-MG collector	Type1287_v2a
Plotters	Type65c/d
Pumps	Type110
Flow mixer	Type11h
Thermostatic 3-way valve	Type11f
Integration block	Type24
Thermostatic control	Equation block
Timer control	Equation block
Water source from the main network	Type14b/Equation block
Variable volume level tank	Type39

The components and their types of the Table 3.1 are explained, as follows, below:

Weather File (Type 15): This file includes all the necessary meteorological data necessary for the entire simulation. It reads the standard hourly data taken at the Larnaca meteorological station and presents for every hour of the year solar angles, irradiance components, ambient and water temperatures, as well as wind speeds and directions.

Water source from the main network (Type 14b/Equation block): These components represent the physical boundary condition of the freshwater supplied in the system. The water supply is regulated according to the model and the necessities of each layout.

V1 PVT-SP collector (Type 1286_v2a): This component is chosen to model the flat-plate WISC collector developed by SolarPeak. It is developed based on the standard ISO 9806:2017 quasi-dynamic efficiency equations and presents the solar heat the V1 PVT-SP collector can extract from the back of the PV panel. This component contains, also, a PID control system that is utilized in the models developed in order to maximize the thermodynamic efficiency of the created thermal hydraulic loops. The PID control system of the component is not visible at the pictures depicting the models and can only be seen at the component's operational details. Its controller functions to modulate pump mass flow rates based on defined temperature setpoint. Thus, for water temperatures below the setpoint of 57,5ºC, the water mass flowrate gets decreased, whereas for temperatures above the setpoint of 57,5ºC, the water mass flowrate gets increased.

V1 PVT-MG collector (Type 1287_v2a): This component is chosen to model the parabolic compound concentrator developed by Double MaReCo. It is configured to handle higher temperature limits (up to 140^{o}C) in order to provide the high-grade thermal boost required for the PEM and alkaline electrolysis configurations. This component contains a PID control system, as well. However, for this collector the PID control system stays inactive utilized for all the layouts that include this type of collector. Once again, the PID control system of the component is not visible at the pictures depicting the models and can only be seen in the component's operational details. Its controller functions to modulate pump mass flow rates based on defined temperature setpoint, exactly like the controller of WISC unit does.

Pumps (Type 110): This component represents variable-speed and fixed-speed circulation pumps. These pumps adjust the mass flow rate passing through the collectors, based on PID control system developed to maintain the temperature of the water close to a setpoint of 57,5^{o}C at the outlet of the V1 PVT-SP collector.

Flow mixer (Type 11h): This component practically models a mixing tank in which two incoming fluid streams are merged into a single outlet. In the TRNSYS models' layouts, it blends colder refilled water from the main supply network with warm water recirculated from the system loop before re-entering the variable volume tank.

Thermostatic 3-way valve (Type 11f): This component acts as an automated water diverter. It has one inlet and two outlets. Based on temperature signals, it determines whether the water has successfully hit the required temperature range (directing it to exit the loop) or if it needs to be recirculated back to the system for further heating.

Variable volume level tank (Type 39): This component models the system's main freshwater tank. Unlike a standard fixed tank, a variable-volume reservoir dynamically computes fluid level rises and drops as water is drawn outside the loop or replenished by the local water supply, preventing lack of water that could lead the pump to run dry or overflow of the tank that could lead to waste of huge amounts of water.

Integration block (Type 24): This block is a computational tracking tool. It integrates instantaneous fluid heat transfer rates and mass flows over the entire simulation year (8760 hours), allowing the calculations of the final total mass of heated water generated at the required temperature ranges.

Thermostatic control (Equation block): This block defines the operational temperature ranges. It serves as a signal that activates or deactivates the 3-way valve based on the thermal needs of each kind of electrolysis.

Timer control (Equation block): This block defines the facility's operational time schedule. It enforces real-life logic by sending an ON/OFF control signal to the circulation pump, limiting its operation to daylight hours, to avoid running the loop at night when no thermal energy can be harvested.

Plotters (65c/d): These components create the necessary graphs presented at the next chapters.

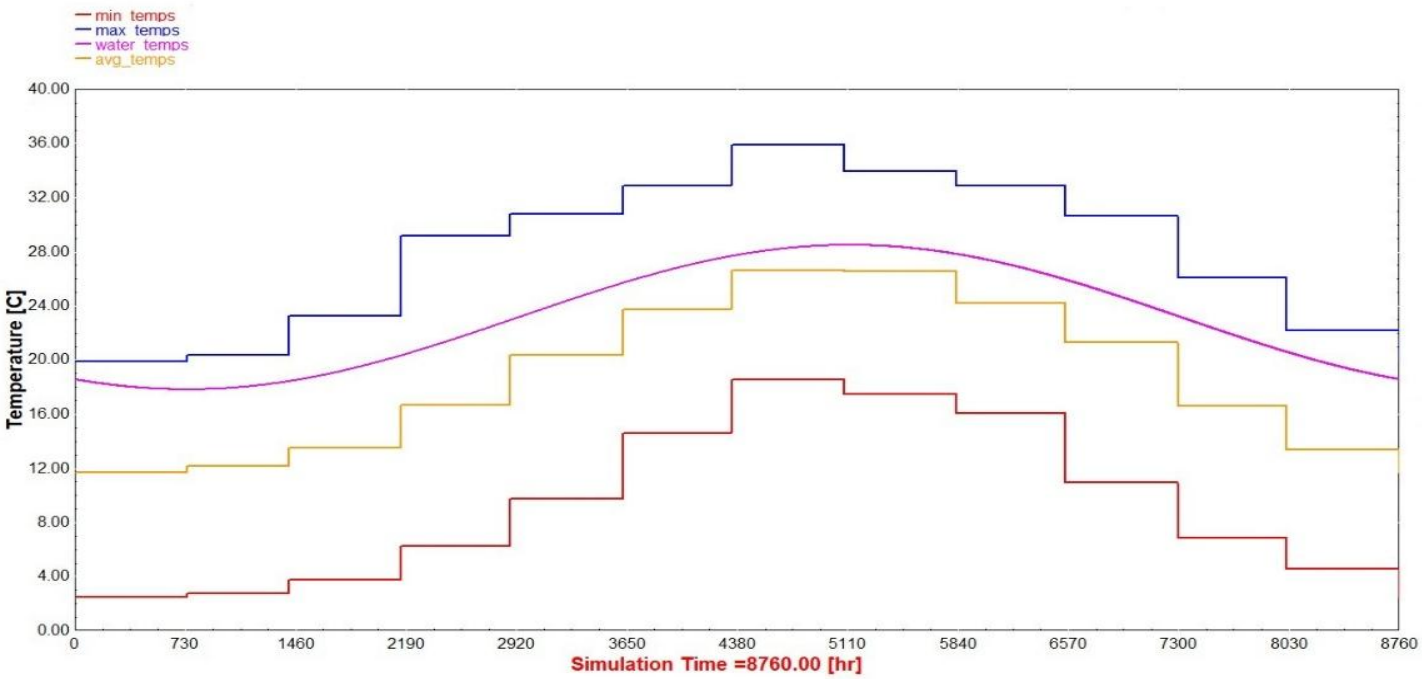

Fig. 3.1: Illustration (made in TRNSYS) of the fresh water, minimum, maximum and average ambient monthly temperatures throughout a year period in Larnaca, Cyprus.

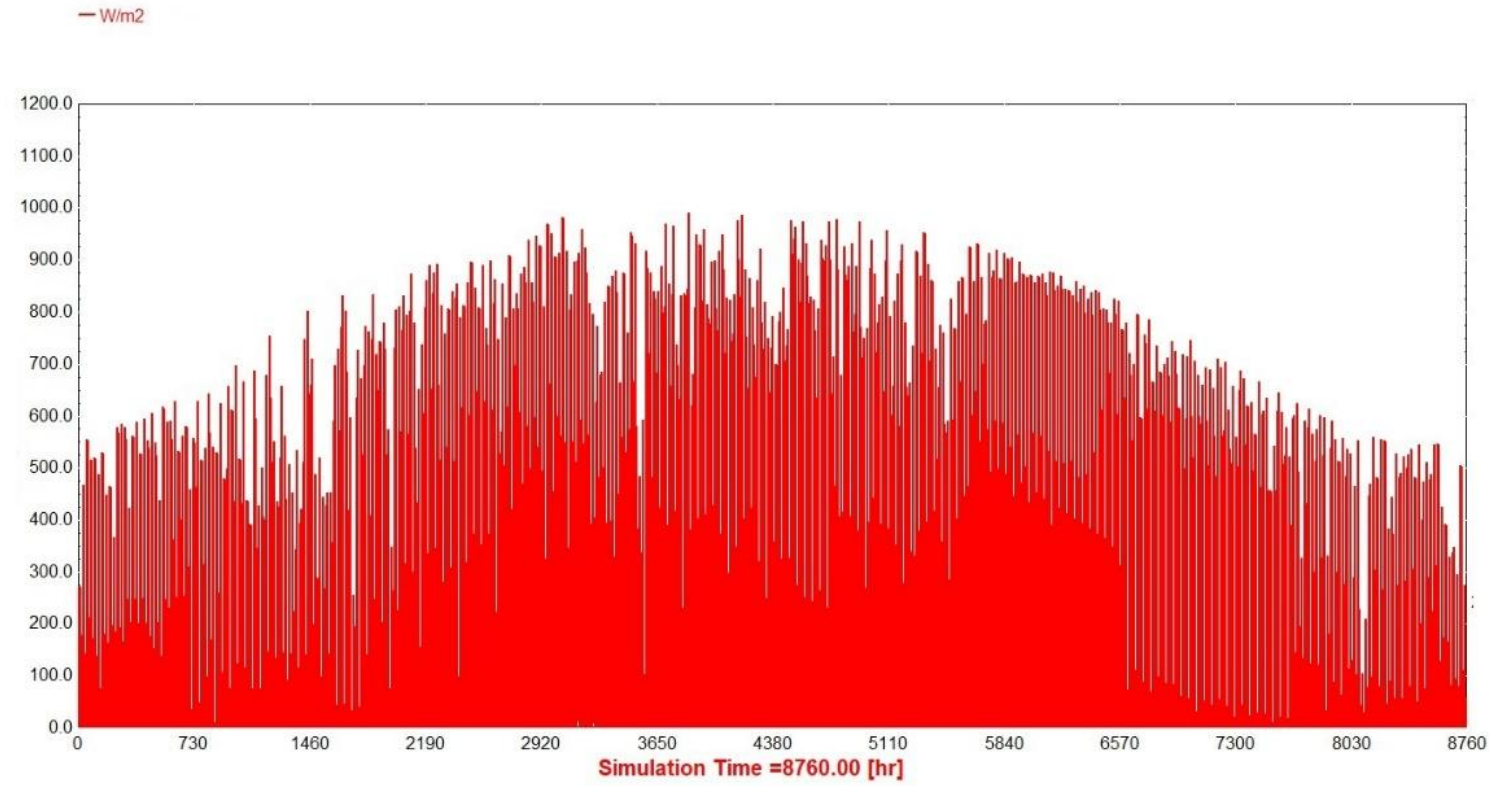

Fig. 3.2: Illustration (made in TRNSYS) of the solar irradiance (in W/m^2) on the horizontal throughout a year period in Larnaca, Cyprus.

As shown in Fig. 3.1 and Fig. 3.2, the southern part of Cyprus is characterized by a warm climate with mild winters and hot summers. Furthermore, the irradiance levels are consistently high, indicating significant potential for the utilization of PVT systems in the region. In Fig. 3.3, below, a simple simulation model is developed to determine the minimum steady-state water flow rate through the V1 PVT-SP collector that ensures the water outlet temperature remains below 60°C, in accordance with the industrial upper-limit specifications.

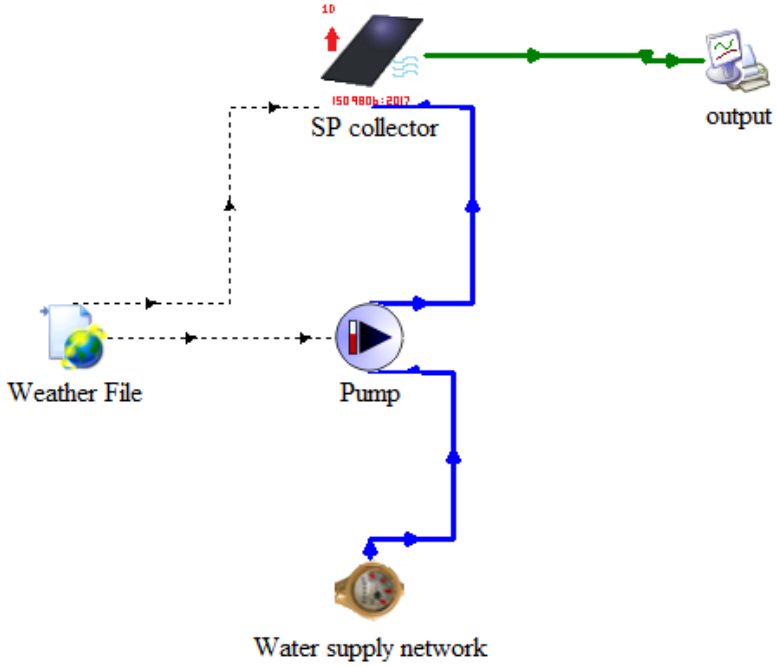

Fig. 3.3: Simplified TRNSYS model of an open loop thermo-hydraulic system simulating the V1 PVT-SP collector that heats water coming from the water supply network.

The connections compiled in TRNSYS models practically equate respective output and input variables, ensuring that fluid parameters (such as water mass flowrates and temperatures) are passed continuously and accurately across components without any numerical losses. The connections made in TRNSYS at the model components of Fig. 3.3 are described and explained below:

Water supply network to Pump

- *Average water draw → Inlet fluid flow rate*

This link connects the local water supply (on-site water source) to the intake of the pump. The "Average water draw" represents the mass flow rate of fresh water needed by the facility over time to satisfy the electrolysis production targets.

Weather File to Pump

- *Mains water temperature → Inlet fluid temperature*

This link connects the local temperature of the freshwater provided from the local supply to the intake of the pump. Practically, it sets the initial temperature of the fresh water at the inlet of the pump.

Pump to V1 PVT-SP collector

- *Outlet fluid temperature → Inlet Temperature*
- *Outlet flow rate → Array Inlet Flowrate*

The first link connects the temperature of the freshwater at the outlet of the pump of the freshwater provided from the local supply to the intake of the pump. The second link connects the water mass flowrate at the outlet of the pump with the water mass flowrate at the inlet of the collector.

Weather File to V1 PVT-SP collector

- *Dry bulb temperature → Ambient Temperature*

This link practically sets the surrounding outdoor air temperature, based on the weather data of the region. The ambient temperature is crucial because the difference between the freshwater temperature flowing inside the collector and the ambient temperature dictates the main part of the continuous convective and conductive thermal heat exchange between the collector and the ambient air.

- *Effective sky temperature → Sky Temperature*

This connection sets the long-wave thermal baseline of the atmospheric sky dome. It enables the model to compute the long-wave infrared radiative exchange, quantifying the rate of radiant heat dissipation from the absorber surface back into the cold upper atmosphere.

- *Wind velocity → Wind Velocity*

This link presents the local wind speed to the collector. It directly influences the heat exchange coefficients of the equation, simulating how rapidly air blowing across a WISC collector speeds up heat dissipation.

- *Total tilted surface radiation for surface → Beam Radiation on the Tilted Surface*

This link is connected with the transfer of direct, unscattered solar rays striking the fixed 25^{o} tilted layout. It is the main driver of peak heat collection for the WISC collector during clear daylight hours.

- *Sky diffuse radiation for surface → Sky Diffuse Radiation on Tilt*

This connection accounts for solar radiation scattered by the atmosphere, clouds and local dust storms. Since the WISC unit is a flat-plate absorber, it collects diffuse light coming from various angles.

- *Ground reflected diffuse radiation for surface → Ground Diffuse Radiation on Tilt*

This connection stands for ground-reflected sunlight. It measures the portion of solar rays that strike at the surrounding ground and facility surfaces, and bounce back reaching the surface of the collectors.

- *Angle of incidence for surface → Incidence Angle*

This input tracks the sun's position relative to the face of your solar panel. The collector model uses this angle to calculate the Incidence Angle Modifier (IAM), which adjusts the system's efficiency because a flat glass surface reflects more sunlight away when the sun strikes it at a sharp, slanted angle.

- *Slope of surface → Collector Slope*

This link sets the fixed physical tilt angle of the array (25°). The tilt angle of the WISC collectors is equal to that of the PV panels.

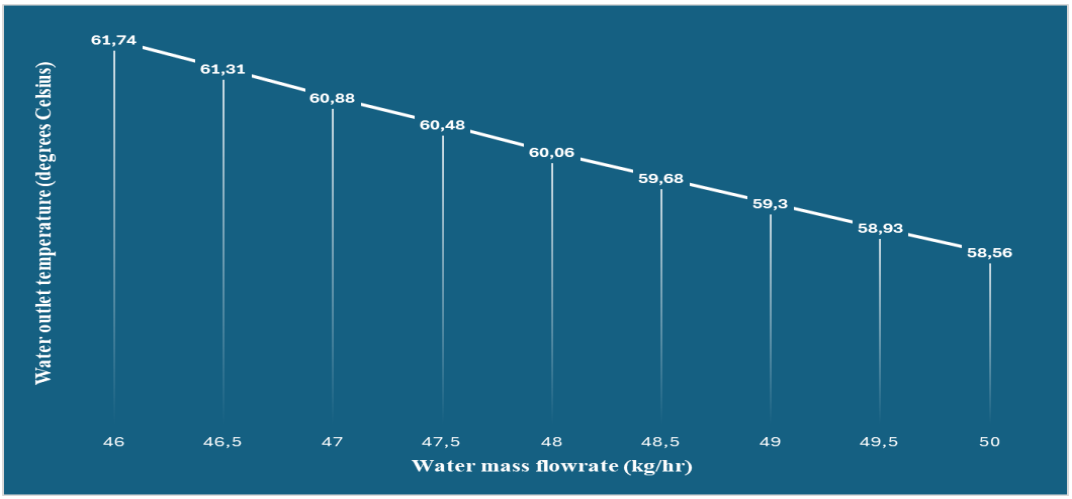

Fig. 3.4: Diagram of the maximum water outlet temperature of the model developed at Figure 3.3 as a function of the water mass flowrate through the V1 PVT-SP collector using a fixed speed pump, based on the simulations made in TRNSYS.

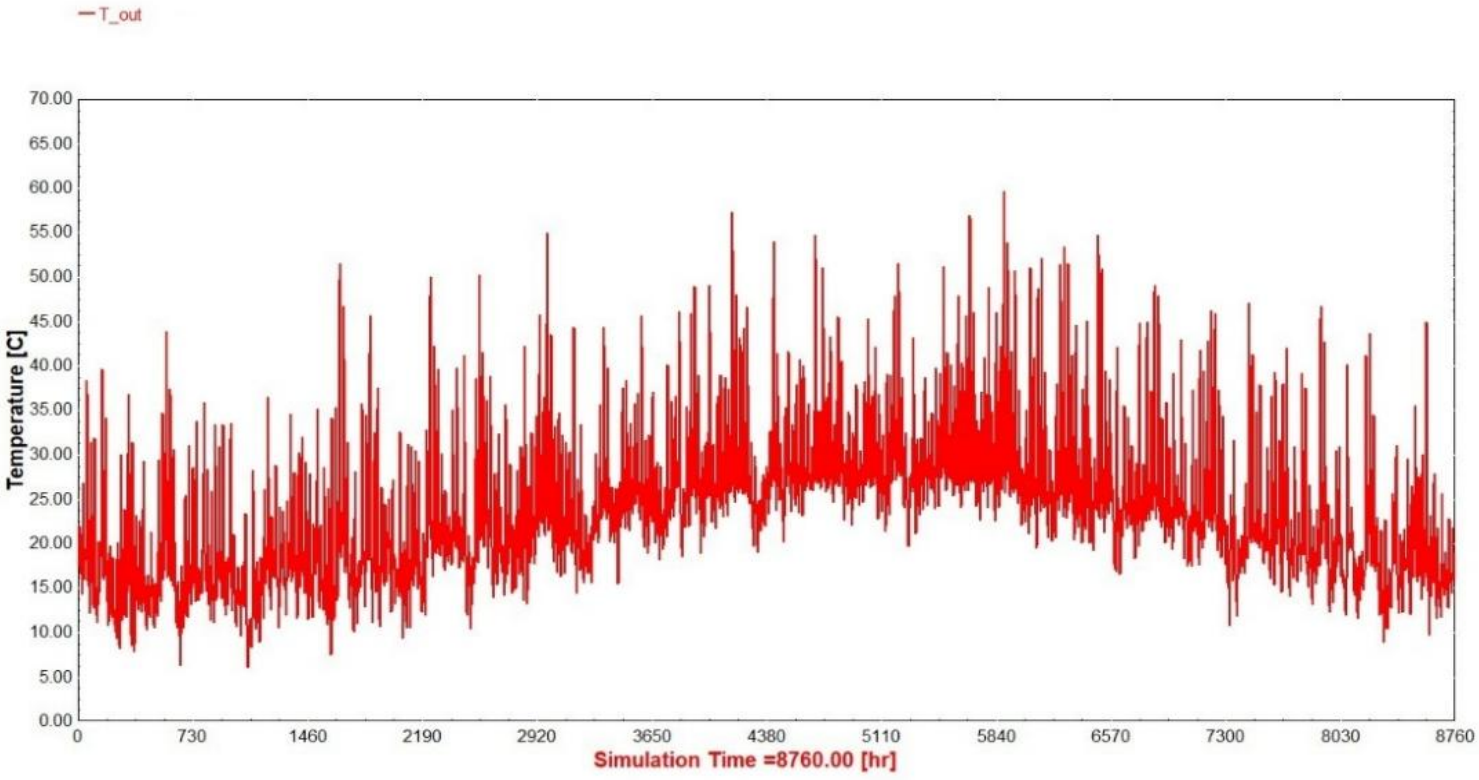

Fig. 3.5: Diagram (made in TRNSYS) of the water outlet temperature throughout the year for a water mass flowrate of 48,5 kg/hr.

As illustrated in Fig. 3.4 and Fig. 3.5, a flow rate of 48,5 kg/hr ensures that the water outlet temperature does not exceed the upper limit of 60°C. However, it should be noted that a steady-state flow rate (a fixed-speed pump) often fails to meet the requirement of heating water to higher temperatures under varying conditions. For this reason, a PID controller is utilized to modulate the water flow rate (integrated into the collector component within the software). The controller aims to maintain the water outlet temperature as close as possible to a setpoint of 57,5°C (2,5ºC below the 60º C limit). Sustaining a high feeding water temperature, enhanced electrolysis efficiency is preserved, thereby minimizing the total electrical energy input required for hydrogen production. By setting the upper limit of the variable-speed pump to 48,5 kg/hr, various simulations were conducted to determine the optimal lower limit. The goal was to identify a minimum flow rate that consistently maintains the temperature below 60°C. As shown in Fig. 3.6, a lower limit of 11,5 kg/hr was identified as the value at which the maximum achieved temperature remains safely below the designated threshold. In Fig. 3.7, it is obvious that for a flowrate range of 11,5-48,5 kg/hr and a PID control system adjusted at an outlet temperature setpoint of 57,5ºC, the simplified model of Fig. 3.3 maintains the water outlet temperature close to 60ºC most of the year period.

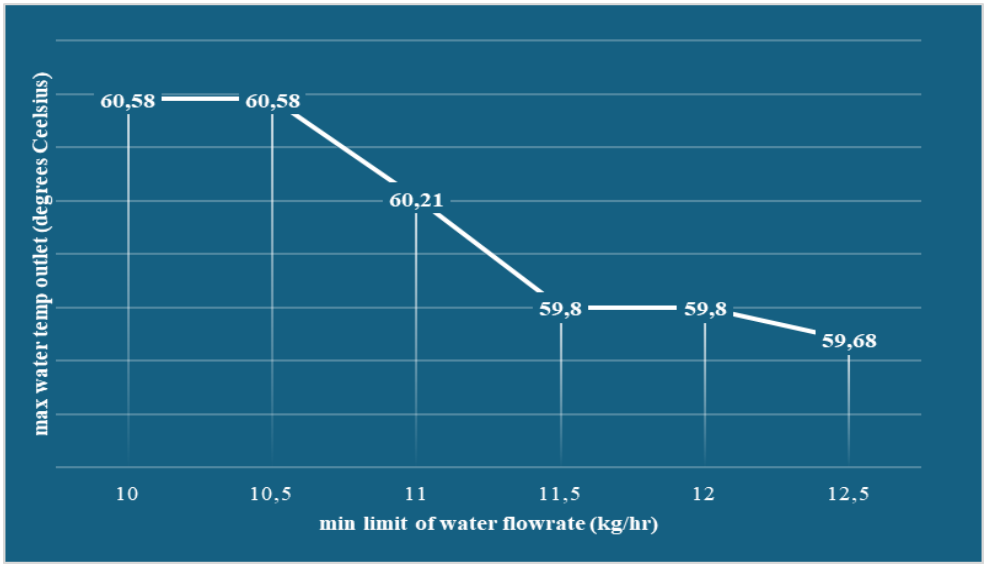

Fig. 3.6: Diagram of the maximum water outlet temperature of the model developed at Fig. 3.3 as a function of a minimum limit for the water mass flowrate through the V1 PVT-SP collector using a variable speed pump with an upper flowrate limit of 48,5 kg/hr, based on the simulations made in TRNSYS.

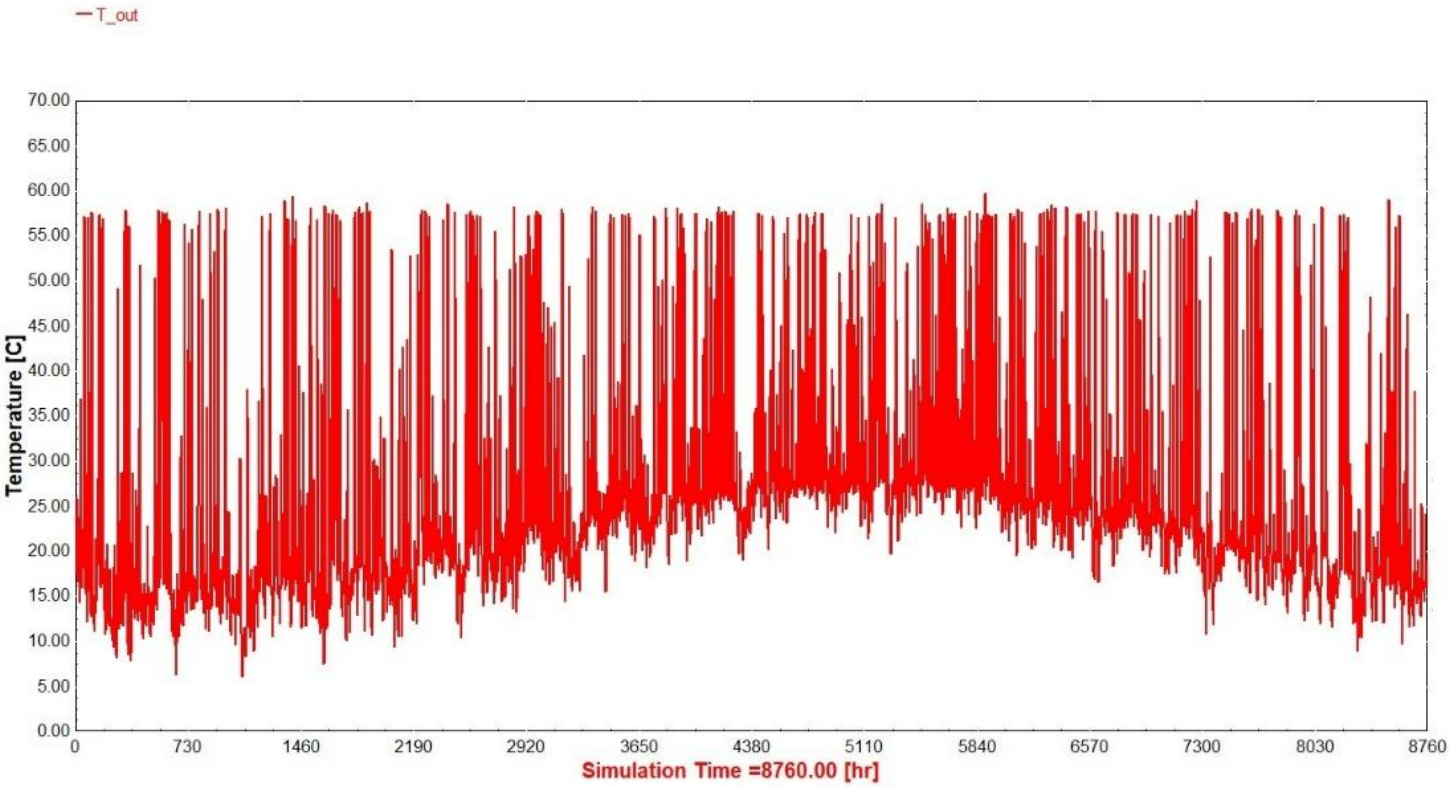

Fig. 3.7: Diagram (made in TRNSYS) of the water outlet temperature at the collector V1 PVT-SP in the model of Fig. 3.3 throughout the year using a variable speed pump that runs in a range between 11,5 and 48,5 kg/hr and a PID control system adjusting the water flowrate in order to maintain a setpoint temperature of 57,5ºC (2,5ºC below the maximum temperature allowed for the specific WISC collector).

In Fig. 3.8, as can be seen, at the model of Fig. 3.3, one V1 PVT-MG collector is added in series as component to determine at which temperatures the water can be heated passing through one V1 PVT-SP collector (at which the utilization of PID control system is active) and afterwards through one V1 PVT-MG collector, which is connected in series and the utilization of its PID control system stays inactive.

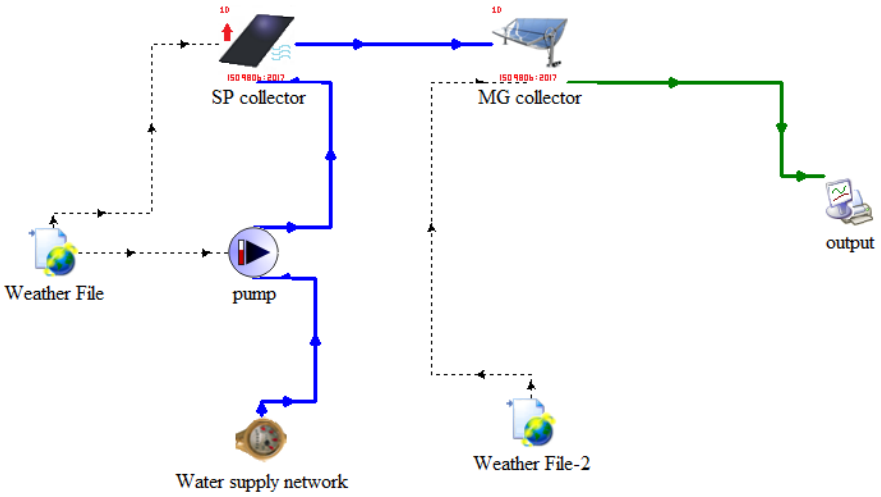

Fig. 3.8: Simplified TRNSYS model of an open loop thermo-hydraulic system including both the V1 PVT-SP and V1 PVT-MG collectors that -connected in series- heat water coming from the water supply network.

To make the model of Fig. 3.8 functionable, some extra connections are made at the model components of TRNSYS, as presented and explained below:

V1 PVT-SP Collector to V1 PVT-MG Collector

- *Outlet Temperature → Inlet Temperature*
- *Outlet Flowrate → Array Inlet Flowrate*

The first link connects the temperature of the freshwater at the outlet of the WISC unit of the freshwater to the inlet of the parabolic collector. The second link connects the water mass flowrate at the outlet of the WISC unit with the water mass flowrate at the inlet of the parabolic collector. These connections ensure the continuous water flow and the absence of heat losses in the process of circulation.

Weather File-2 to V1 PVT-MG Collector

- *Dry bulb temperature → Ambient Temperature*
- *Effective sky temperature → Sky Temperature*
- *Wind Velocity → Wind Velocity*
- *Beam radiation for surface → Beam Radiation on the Tilted Surface*
- *Sky diffuse radiation for surface → Sky Diffuse Radiation on Tilt*
- *Ground reflected diffuse radiation for surface → Ground Diffuse Radiation on Tilt*
- *Angle of incidence for surface → Incidence Angle*
- *Slope of surface → Collector Slope*

As can be seen, the connection between the second weather file and the parabolic collector is the same as the ones between the first weather file and the WISC unit at the previous model. However, in this case the only thing that changes is the parabolic collector's slope which, as shown next, is different to the one of the WISC units.

As demonstrated in various studies, the optimal collector slope for maximum annual energy availability is typically equal to the local latitude in low-latitude regions (<40^{o}) (Skerlic et al., 2018). By performing simulations of the model presented in Fig. 3.9, diagrams of the average water outlet temperatures were generated for each month (as shown in Fig. 3.10). The results indicate that tilt angles that are lower than the region's latitude (approximately 35^{o} in this case) yield slightly higher temperatures during the spring and summer months. Conversely, tilt angles that are higher than the latitude result in higher temperatures during the autumn and winter. Therefore, selecting a collector slope of 35^{o} is a reliable, balanced option, as there is no specific requirement to prioritize a particular season. For the simulations involving two collector types, separate weather files were used to define the slopes: 25^{o} for the V1 PVT-SP collector and 35^{o} for the V1 PVT-MG collector. Based on simulations made in the model of Fig. 3.9 for the angle values stated before and as illustrated on Fig. 3.10, the water can be heated up to 140°C, which remains consistent with its industrial specifications.

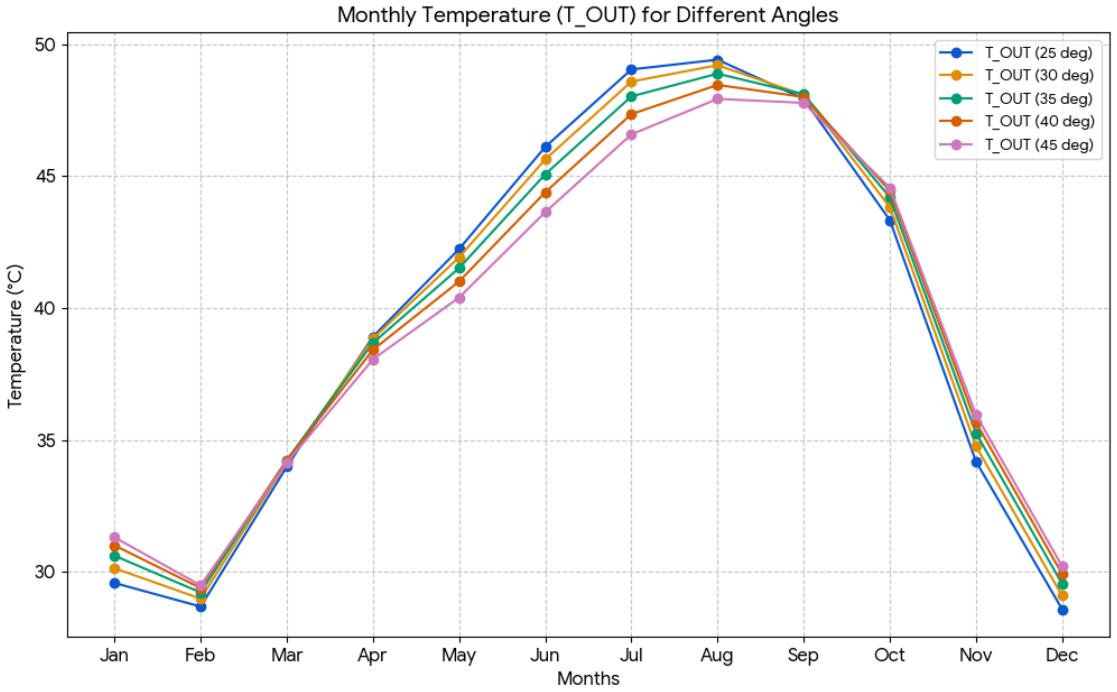

Fig. 3.9: Diagram (based on results of TRNSYS simulations of the model in Fig. 3.8) of the monthly average water outlet temperatures of the V1 PVT-MG collector throughout the year, for different values of V1 PVT-MG collector's slope and for a pump working all year long without any pause.

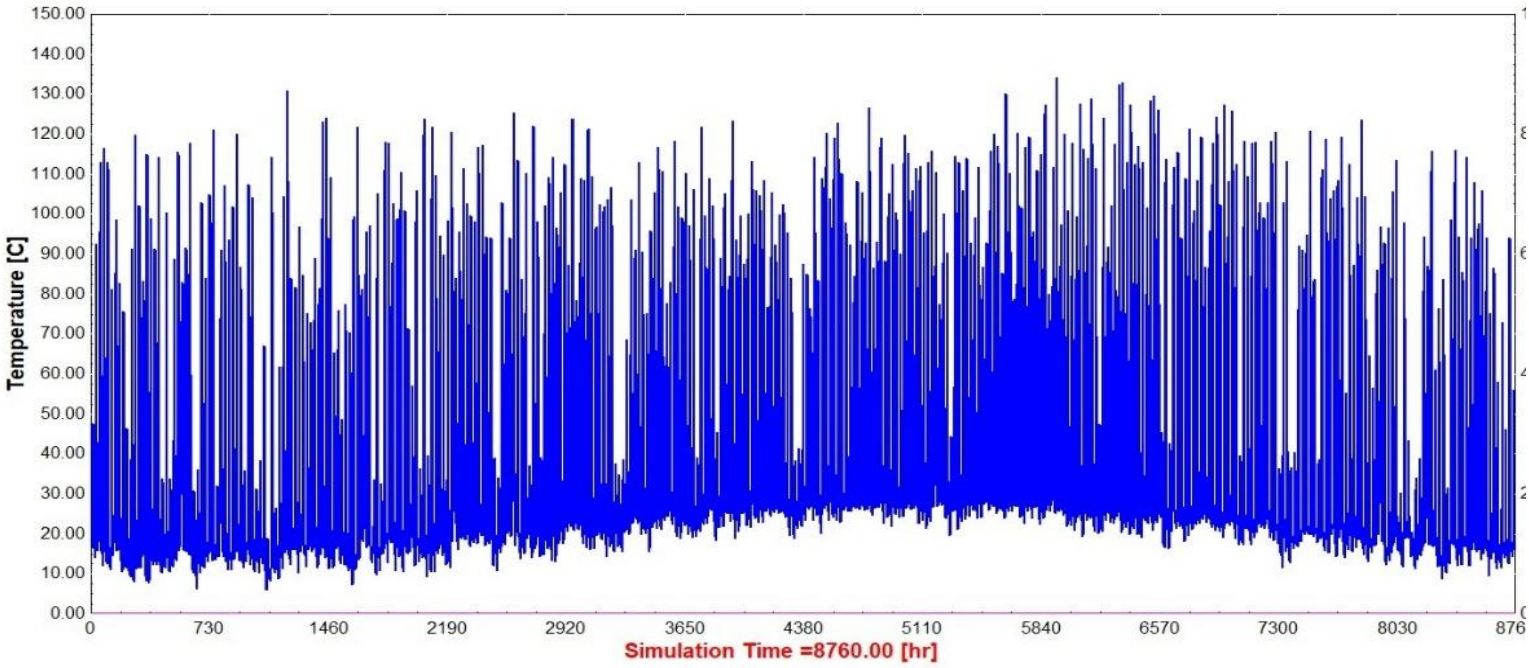

Fig. 3.10: Diagram (made in TRNSYS) of the water outlet temperature of the V1 PVT-MG collector in the model of Fig. 3.8, throughout the year for a slope of the parabolic collector equal to 35°.

3.1. Water heating for AEM Electrolysis (40º-60ºC)

For this study, a TRNSYS model was developed based on a single-type collector case, as the V1 PVT-SP collector can achieve water outlet temperatures within the 40°C to 60°C range. The model, illustrated in Fig. 3.1.1, was constructed according to the methodology previously described as single collector model.

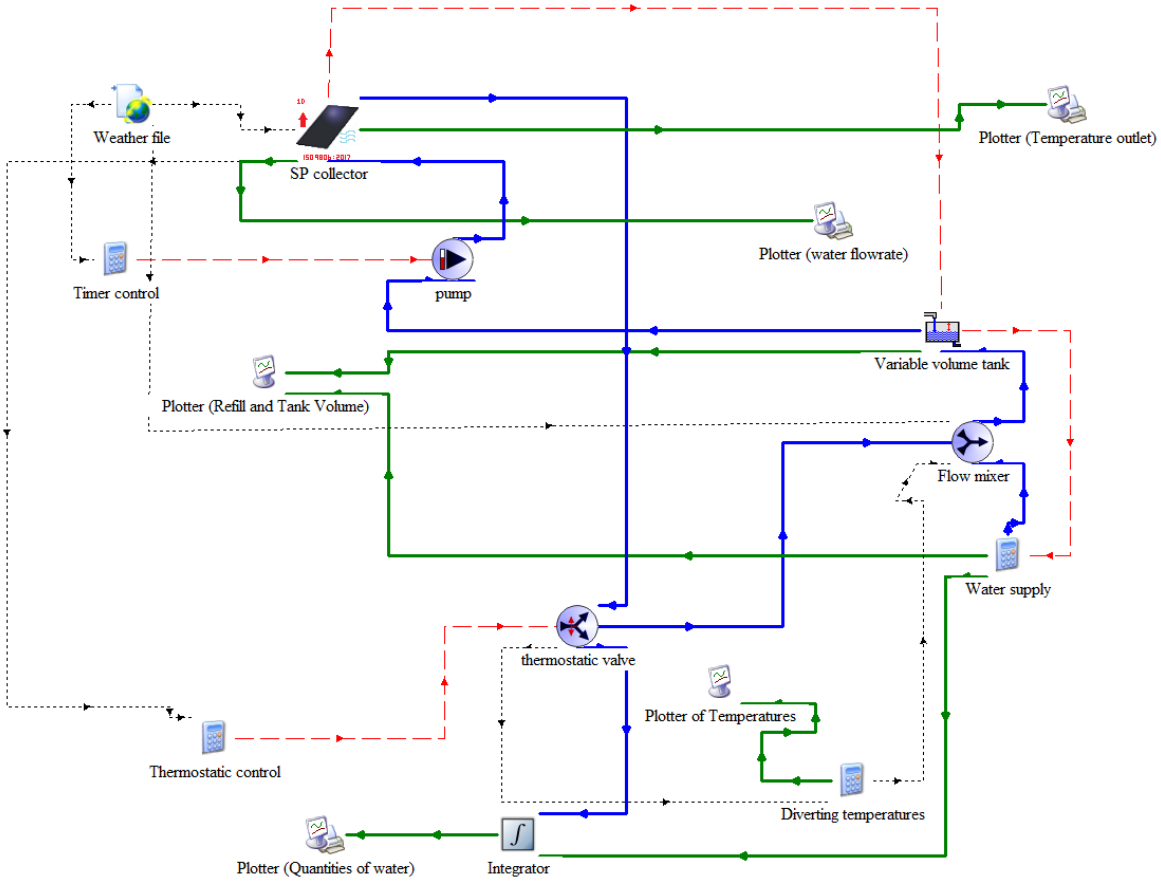

Fig. 3.1.1: TRNSYS model of a closed loop thermo-hydraulic system using the V1 PVT-SP collector for the generation of heated water at temperatures above 40ºC and as close as it gets to 60ºC without exceeding that limit. This model is used only for the operational temperature range of AEM method of electrolysis.

Apart from connections made on the two precious simplified models, which remain the same for the model of Fig.3.1.1, some additional connections are made and they are presented and explained below:

Water Flow

Water Supply to Flow Mixer

- *M_refill → Flow rate at inlet 1*

This link represents the refilling of freshwater at the variable volume tank of the closed-loop system, every time that the level of the tank reaches a certain point. Between the local water supply and the tank, the refilled water passes through a flow mixer that merges the two flows coming from the water supply and the thermostatic 3-way valve of the closed-loop network.

Flow Mixer to Variable Volume Tank

- *Outlet temperature → Inlet temperature*
- *Outlet flow rate → Inlet flow rate*

These two links ensure the continuous water flow and the absence of heat losses in the process of circulation, between the flow mixer and the tank. The temperature of the water coming out of the mixer is dependent on the conditions of the two flows that get in it, whereas the water flowrate at the outlet of the mixer is the sum of the two flowrates in the two inlets of the mixer, as shown at the two equations below.

Mass equilibrium of the flow mixer: $\dot{m}_{out} = \dot{m}_{in,1} + \dot{m}_{in,2}$ [eq.10]

Thermal equilibrium without thermal losses through the flow mixer:

$$T_{out} = \frac{\dot{m}_{in,1} T_{in,1} + \dot{m}_{in,2} T_{in,2}}{\dot{m}_{in,1} + \dot{m}_{in,2}}$$ [eq.11]

Variable Volume Tank to Pump

- *Fluid temperature → Inlet fluid temperature*
- *Load flow rate → Inlet fluid flow rate*

The first link ensures the absence of heat losses between the tank and the pump, whereas the "Load flow rate" is the specific value the volume of water has that the closed-loop water flow process needs to pull out of the tank at that exact moment. Thus, the second link ensures the continuous water flow in this case.

Pump to V1 PVT-SP Collector

- *Outlet fluid temperature → Inlet Temperature*
- *Outlet flow rate → Array Inlet Flowrate*

As explained in previous model, these two connections ensure the continuous water flow and the absence of heat losses in the waterflow between the pump and the WISC unit.

V1 PVT-SP collector to Thermostatic Valve

- *Outlet Temperature → Inlet temperature*
- *Outlet Flowrate → Inlet flow rate*

These two connections ensure the continuous water flow and the absence of heat losses in the waterflow between the WISC unit and the 3-way thermostatic valve.

Thermostatic Valve to Flow Mixer

- *Flow rate at outlet 1 → Flow rate at inlet 2*

This connection presents the basic function of the thermostatic valve. The "Flow rate at outlet 1" is the water flowrate at time periods that the water does not reach the required temperature range and thus is directed at one of the two inlets of the flow mixer, instead of exiting the closed-loop system and utilized for electrolysis process.

SP collector to Thermostatic Control

- *Outlet Temperature → T_out*

This link sends the value of the water temperature at the outlet of the WISC unit at thermostatic control, in order to act as a signal and direct the water where necessary, either out of the loop or back to the closed-loop system.

Weather File to Flow mixer

- *Mains Water Temperature → Temperature at inlet 1*

This connection sets the temperature of the refilled water equal to the temperature of the water coming from the local water supply.

Weather File to Timer Control

- *Hour of the day → Day_hour*

This connection works as a clock since it presents what time is, throughout the day. As explained below, this value is sent afterwards from timer control to pump and works as an ON/OFF signal.

Signal lines

Thermostatic Control to Thermostatic Valve

- *Ctrl_signal → Control signal.*

This link allows the equation component to dictate the flow ratio (practically ON/OFF) in the diverting valve. The output from the Thermostatic Control equation block has the function "*Ctrl_signal=gt(40,T_out)*", meaning that the valve is activated when the temperature is above 40^{o}C.

Timer Control to Pump

- *ss_pp_ctrl → Control signal.*

This link sends a control signal (ON/OFF) to the circulation pump. This way, the pump operates during the hours of the day so that the system can be efficient. Specifically, the output from the Timer Control equation block has the function "*and(gt(Day_hour, 7),lt(Day_hour,20))*", meaning that the pump operates from 7 a.m to 8 p.m, every day.

Variable Volume Tank to Water Supply

- *Fluid volume → Vol.*

This link feeds a signal with the current volume level of the tank back into an equation block that defines when the tank is refilled in a way that never gets empty or overflown. In this case, the Water Supply equation block has the function "*M_refill=LT(Vol,0.3)*1500*", meaning that every time that the tank's volume level falls below 300 liters the water supply from the main network is activated and the tank gets 1500 liters in an hour. This way, the volume of the tank remains always at an intermediate level without causing any concern.

V1 PVT-SP Collector to Variable Volume Tank

- *Outlet Flowrate → Flow rate to load.*

This specific connection suggests that the heated water flowrate from the collector is being treated as the "load" supply for the tank component.

Table 3.1.1: Table of values used for the simulation of the model of Fig.3.1.1.

Overall Tank Volume	2 m^3
Minimum Fluid Volume (low level alarm)	0,1 m^3
Maximum Fluid Volume (high level alarm)	1,9 m^3
Initial Fluid Volume	1,5 m^3
Specific Heat Capacity (c_p)	4,19 KJ/kg.K
Water density	1000 kg/m^3

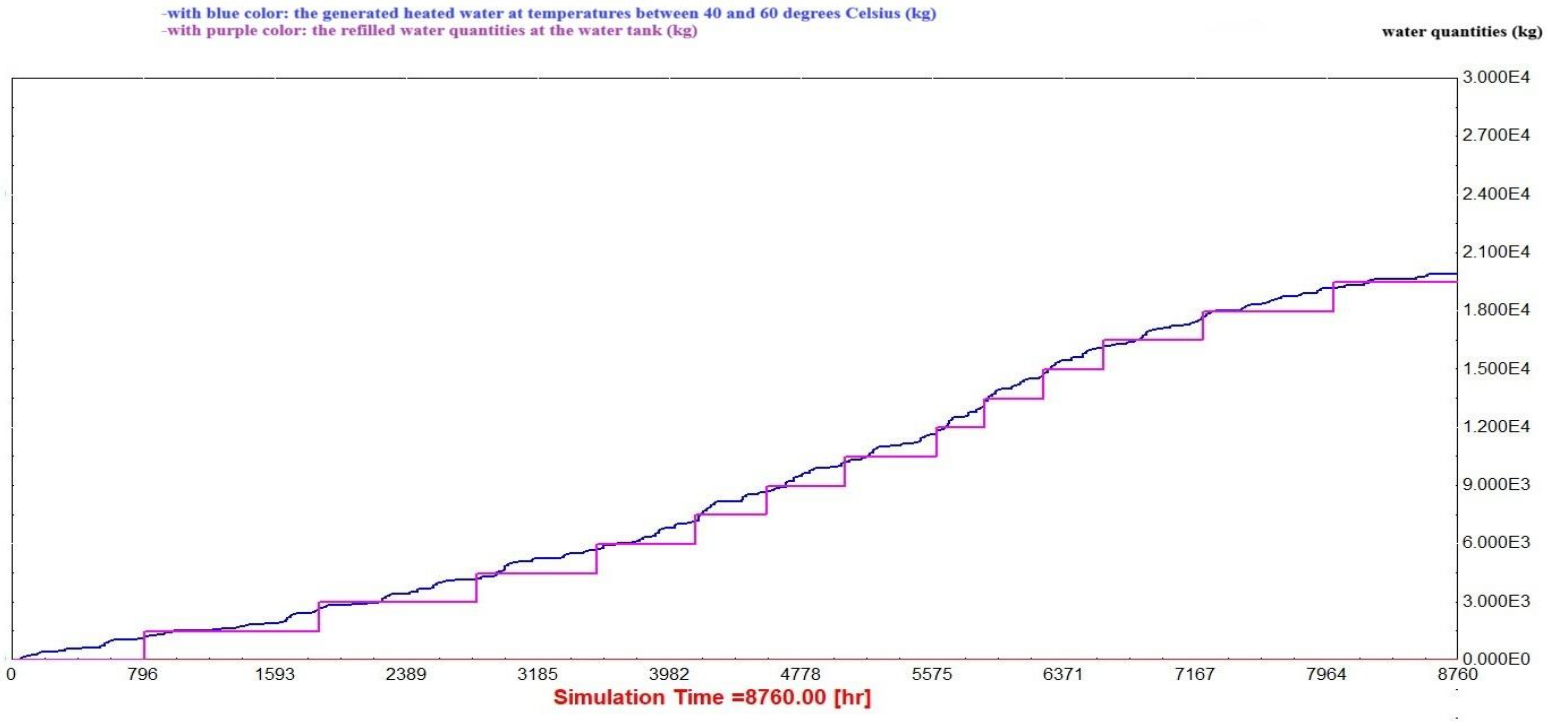

Fig. 3.1.2: Diagram (made in TRNSYS) produced by the simulations of the model of the Fig.3.1.1, showing the heated water generated between 40^{o} and 60^{o}C as well as the refilled water quantities in the tank throughout the year

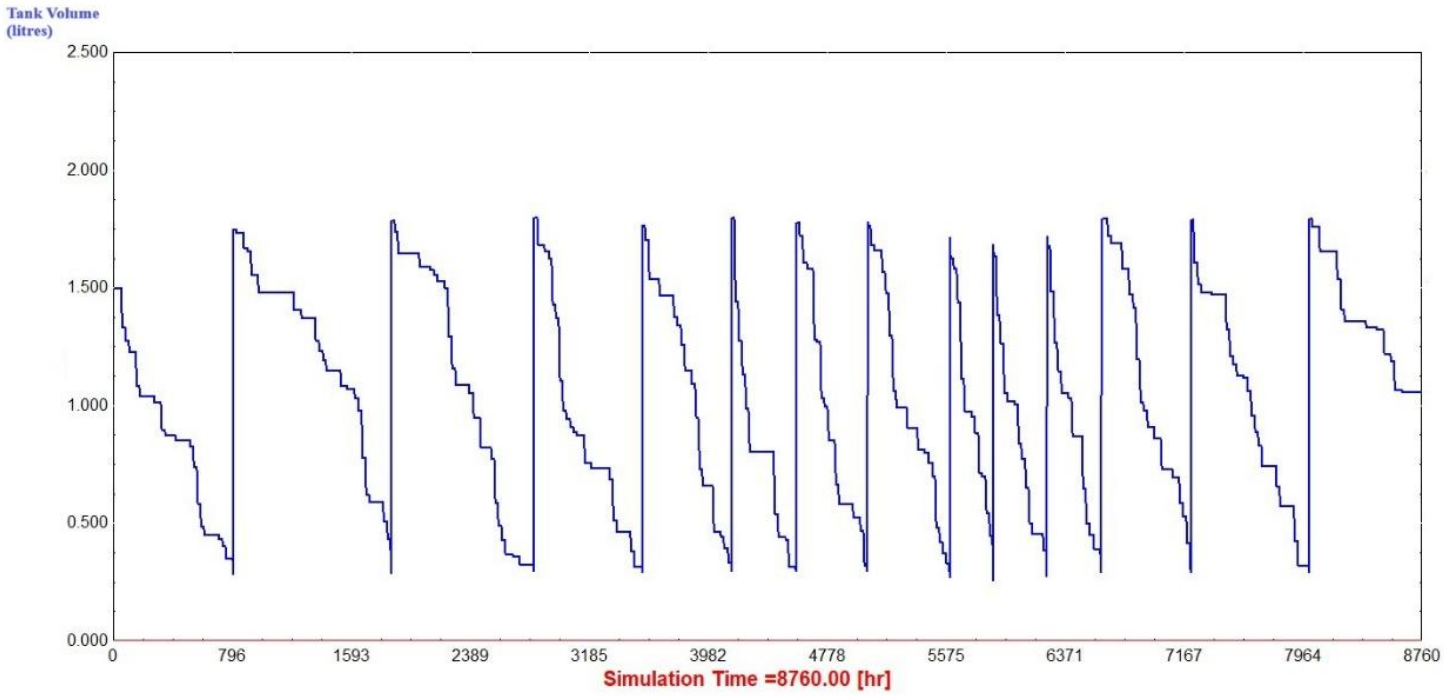

Fig. 3.1.3: Diagram (made in TRNSYS) produced by the simulations of the model 3.1.1, showing the water volume level in the tank throughout the year.

Table 3.1.2: Table of results from the simulation of the model of Fig. 3.1.1, including one V1 PVT-SP collector, based on the assumptions made previously at the chapter.

heated water produced at 40-60 deg. Celsius (kg)	19.500
water refilled in the tank (kg)	19.944
water left in the tank (kg)	1.056

As can be seen in the graphs presented above, the simulations present realistic operational behavior and the tank is refilled correctly according to the control command given, whereas the water outlet temperature does not ever exceed the limit of 60ºC.

3.2. Water heating for PEM Electrolysis (50º-90ºC)

For this study, a TRNSYS model was developed based on a dual-type collector scenario, as the V1 PVT-SP collector cannot achieve water outlet temperatures above 60°C and the use of the V1 PVT-MG collector becomes necessary. The model, illustrated in Fig. 3.2.1, was constructed according to the methodology previously described for the two collectors' model. The same model is also applied for the case of alkaline electrolysis which needs an operational temperature range between 70º and 90ºC. The model of Fig. 3.2.1 is slightly modified compared to the one of Fig. 3.1.1, to include the V1 PVT-MG collector. On this model, various layouts are applied with one and more WISC collectors connected in parallel and all of them connected in series with one parabolic collector.

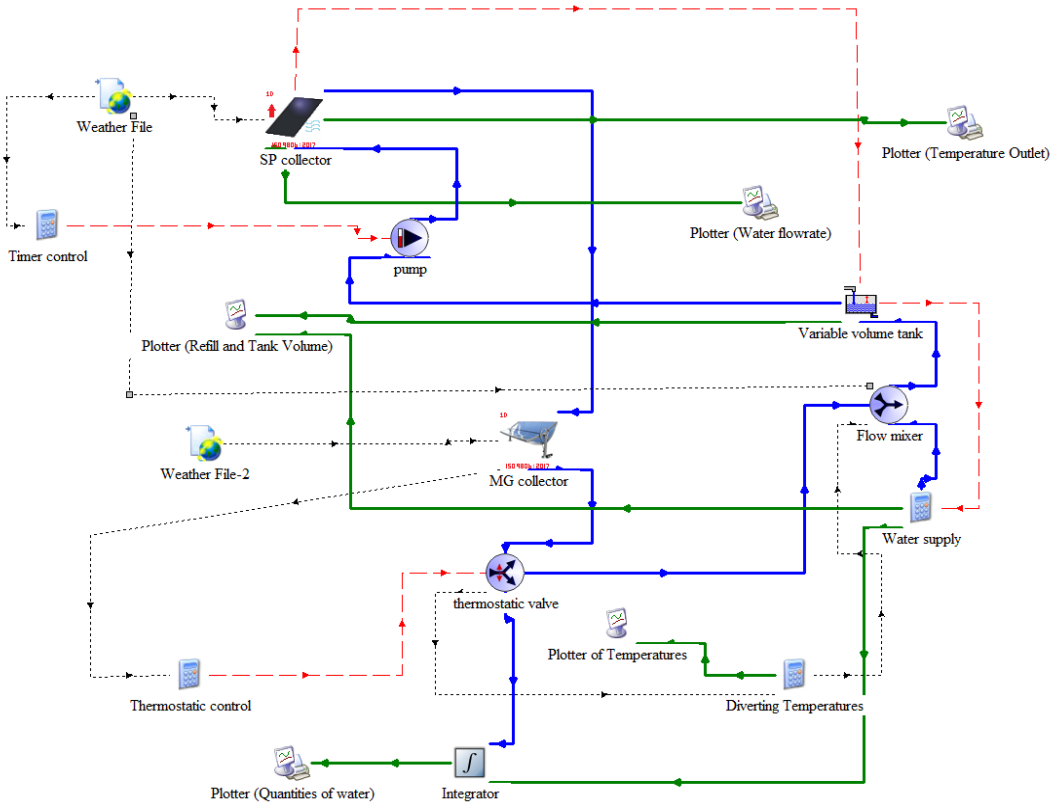

Fig. 3.2.1: TRNSYS model of a closed loop thermo-hydraulic system using both the V1 PVT-SP and V1 PVT-MG collectors for the generation of heated water at temperatures above 50ºC or 70ºC and till 90ºC. This model is used for the operational temperature ranges of both PEM and alkaline methods of electrolysis.

Most of the connections made in the model of Fig. 3.2.1 are the same with the ones made in the model of Fig. 3.1.1. The only ones that are changed are the ones between the V1 PVT-SP collector(s) and the thermostatic valve, and they are presented below:

V1 PVT-SP to V1 PVT-MG

- *Outlet Temperature → Inlet Temperature*
- *Outlet Flowrate → Array Inlet Flowrate*

These two connections ensure the continuous water flow and the absence of heat losses in the waterflow between the WISC unit and the parabolic collector.

V1 PVT-MG to Thermostatic valve

- *Outlet Temperature → Inlet Temperature*
- *Outlet Flowrate → Inlet Flowrate*

These two connections ensure the continuous water flow and the absence of heat losses in the waterflow between the parabolic collector and the thermostatic valve.

The Thermostatic Control equation block has the function "*Ctrl_signal=gt(50,T_out)*", meaning that the valve is activated when the temperature is above 50ºC. However, in some cases, mentioned at layouts below, another function is used to keep the temperature in a range between 50ºC and 90ºC. This function is "*Ctrl_signal=and(gt(50,T_out),lt(90,T_out)*" and practically acts as a "dual action" thermostatic valve deactivated when the water temperature is below 50 ºC and above 90ºC.

1 SP collector and 1 MG collector in series

Table 3.2.1: Table of initial values used for the simulation of the model of Fig. 3.2.1. including one V1 PVT-SP and one V1 PVT-MG collectors in series.

Overall Tank Volume	10,0 m^3
Minimum Fluid Volume (low level alarm)	0,1 m^3
Maximum Fluid Volume (high level alarm)	9,9 m^3
Initial Fluid Volume	9,0 m^3
Specific Heat Capacity (c_p)	4,19 KJ/kg.K
Water density	1000 kg/m^3

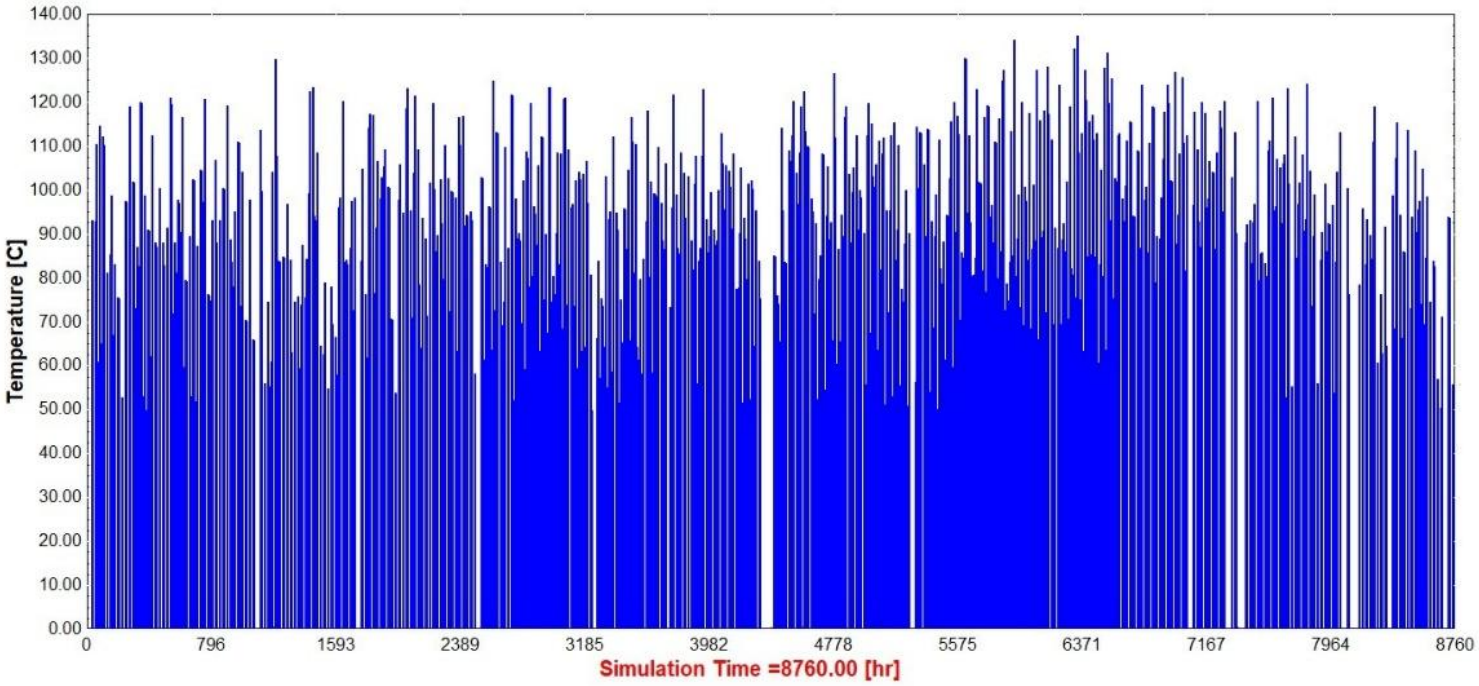

Fig. 3.2.2: Diagram (made in TRNSYS) based on simulations of the model of Fig. 3.2.1., including one V1 PVT-SP and one V1 PVT-MG collectors in series, depicting the hours of the year that water flow temperature exceeds 50ºC and it is directed outside the closed-loop system.

As demonstrated in the diagram above, the outlet temperatures frequently exceed 90°C, which is the upper operating limit for the PEM electrolysis process. To address this issue, a dual-action thermostatic valve (configured to open at 50°C and close at 90°C) was implemented. Furthermore, adjustments were made to increase both the storage tank volume and the freshwater replenishment rates. However, despite the use of the thermostatic valve to regulate the output range, the water outlet temperature from the V1 PVT-SP collector still frequently exceeds 60°C, occasionally reaching above 70°C. Moreover, increasing the tank volume (even to significantly larger dimensions) proved insufficient in lowering the temperatures to the required levels. So, studying models of more than one V1 PVT-SP collectors in parallel with one V1 PVT-MG collector in series turns out to be a better option. As elaborated in the next chapter focusing on alkaline electrolysis operational temperature range, this layout requires an expanded flow rate range that is significantly higher than the limits defined previously.

2 SP collectors in parallel and 1 MG collector in series

Table 3.2.2: Table of values used for the simulation of the model of Fig. 3.2.1, including two V1 PVT-SP collectors in parallel and one V1 PVT-MG collector in series.

Overall Tank Volume	6,5 m^3
Minimum Fluid Volume (low level alarm)	0,1 m^3
Maximum Fluid Volume (high level alarm)	6,4 m^3
Initial Fluid Volume	5,0 m^3
Specific Heat Capacity (c_p)	4,19 KJ/kg.K
Water density	1000 kg/m^3

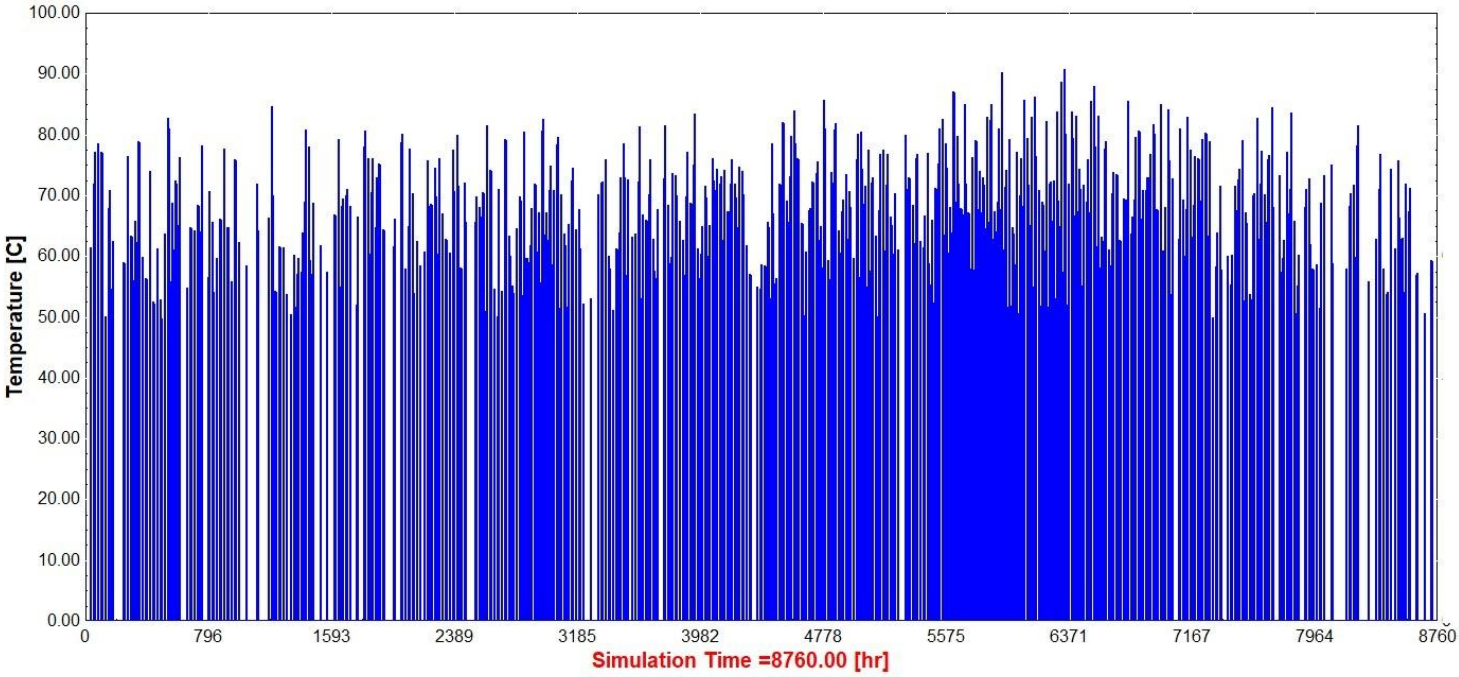

Fig. 3.2.3: Diagram (made in TRNSYS) based on simulations of the model of Fig. 3.2.1., including two V1 PVT-SP collectors in parallel and one V1 PVT-MG collectors in series, depicting the hours of the year that water flow temperature exceeds 50ºC and it is directed outside the closed-loop system.

As noted on Fig. 3.2.3, the temperature values in this layout are more limited compared to those of the previous layout. However, the utilization of a "dual action" thermostatic valve that opens at 50ºC and closes at 90ºC must be applied to limit the upper temperature limit at 90ºC.

with "dual-action" thermostatic valve

In this case, the Water Supply equation block has the function "*M_refill=LT(Vol,1.5)*4800*", meaning that every time that the tank's volume level falls below 1500 liters the water supply from the main network is activated and the tank gets 5000 liters in an hour. The output from the Thermostatic Control equation block has the function "*Ctrl_signal=and(lt(90,T_out),gt(50,T_out))*".

Table 4.2.3: Table of values used for the simulation of the model of Fig. 3.2.1, including two V1 PVT-SP collectors in parallel and one V1 PVT-MG collector in series with a thermostatic valve that does not permit the water that exits the loop to surpass the limit of 90ºC.

Overall Tank Volume	6,5 m^3
Minimum Fluid Volume (low level alarm)	0,1 m^3
Maximum Fluid Volume (high level alarm)	6,4 m^3
Initial Fluid Volume	5,0 m^3
Specific Heat Capacity (c_p)	4,19 KJ/kg.K
Water density	1000 kg/m^3

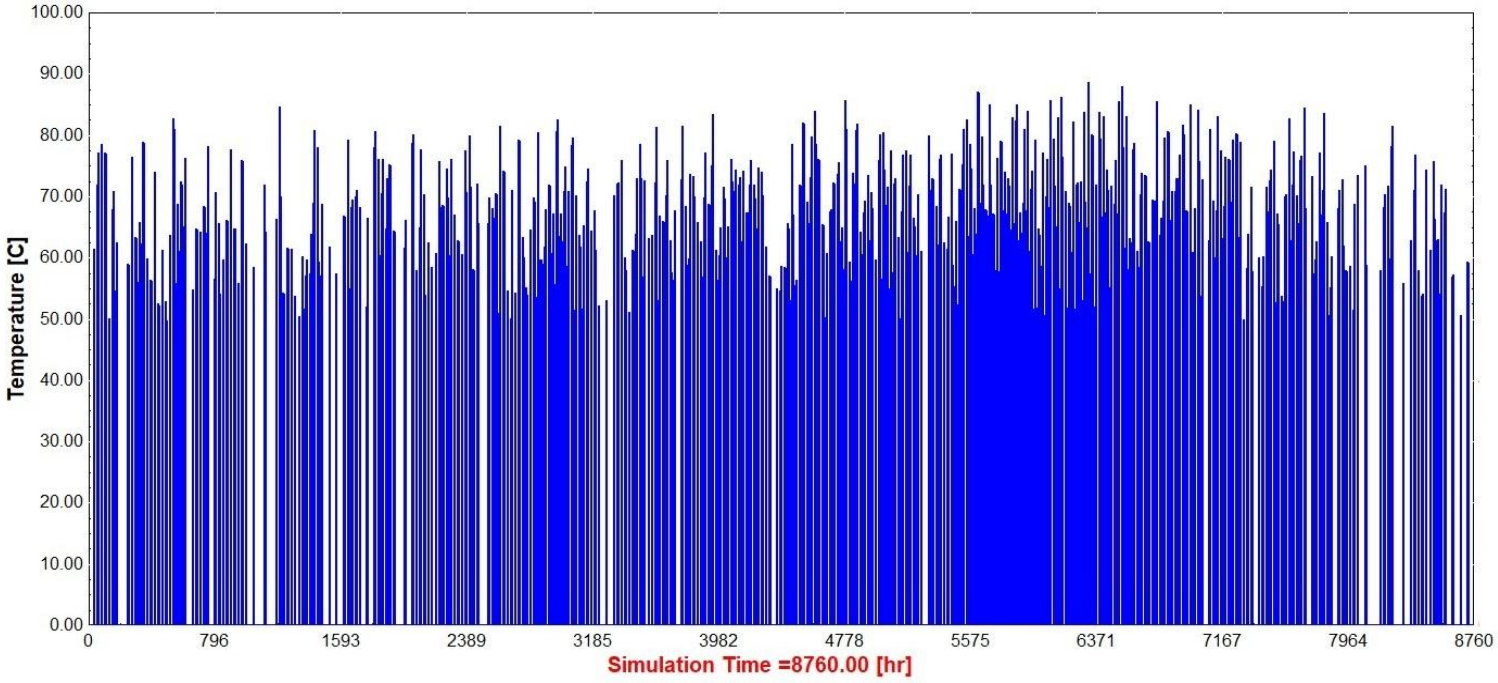

Fig. 3.2.4: Diagram (made in TRNSYS) based on simulations of the model of Fig. 3.2.1., including two V1 PVT-SP collectors in parallel and one V1 PVT-MG collectors in series, with the utilization of a "dual action" thermostatic valve, depicting the hours of the year that water flow temperature is between 50ºC and 90ºC, and it is directed outside the closed-loop system

.

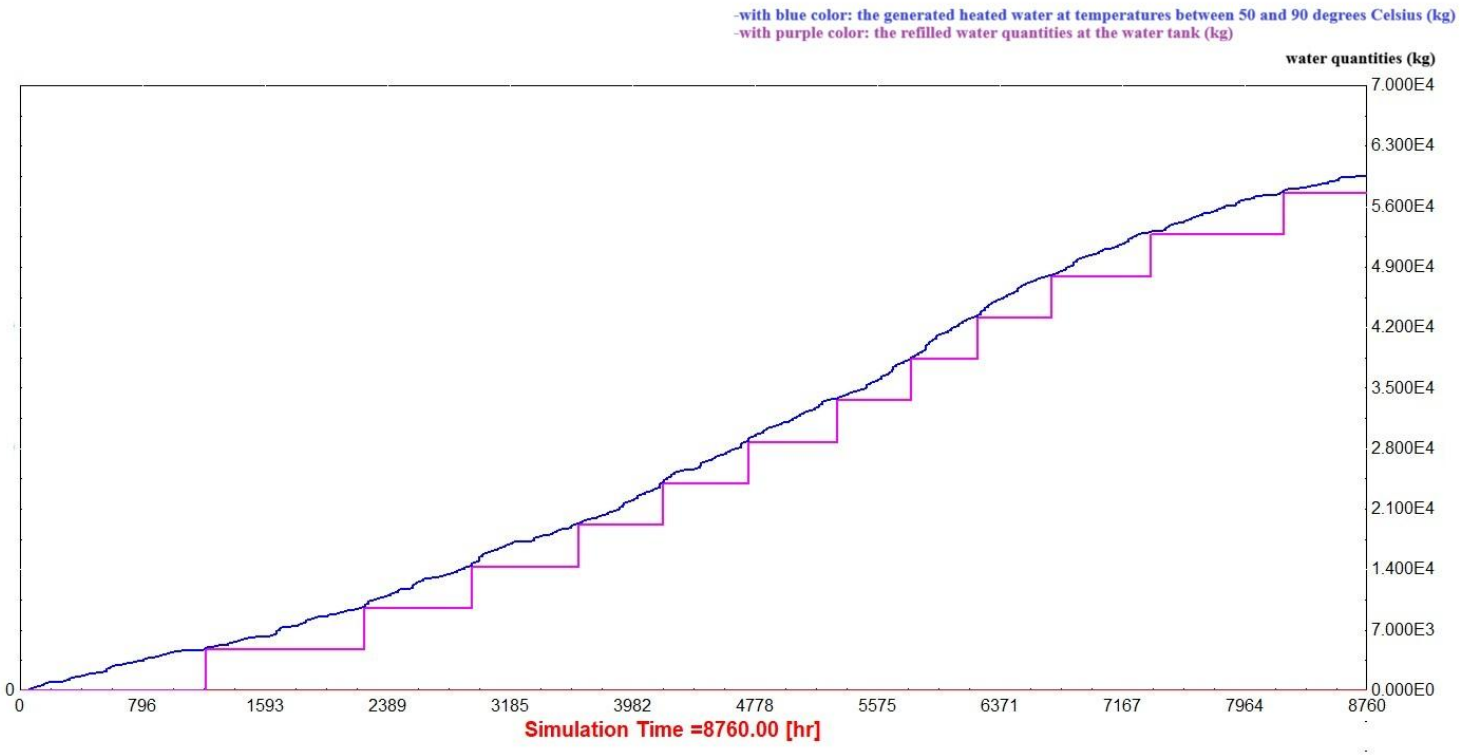

Fig. 3.2.5: Diagram (made in TRNSYS) produced by the simulations of the model of the Fig.3.1.1, including two V1 PVT-SP collectors in parallel and one V1 PVT-MG collectors in series, with the utilization of a "dual action" thermostatic valve, showing the heated water generated between 50^{o} and 90^{o}C as well as the refilled water quantities in the tank throughout the year

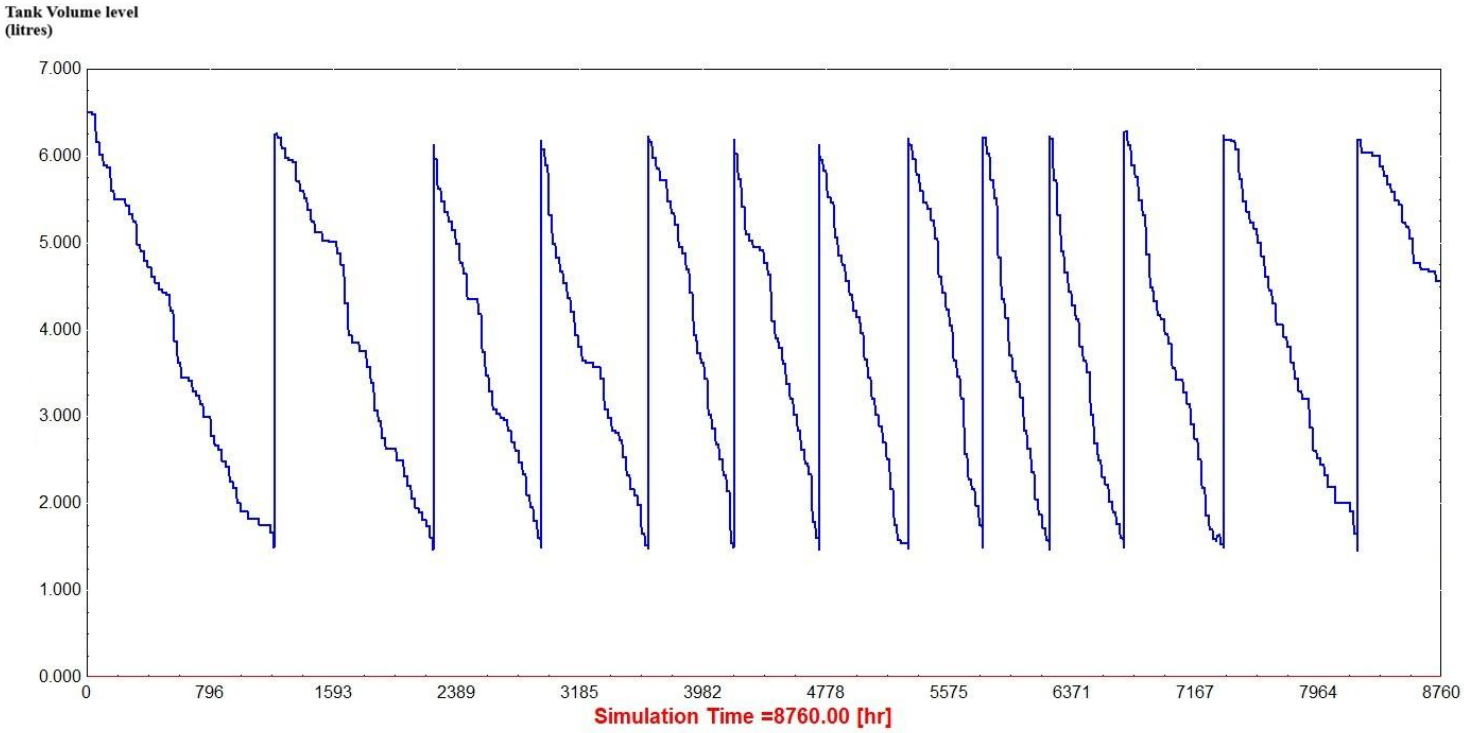

Fig. 3.2.6: Diagram (made in TRNSYS) produced by the simulations of the model 3.2.1, including two V1 PVT-SP collectors in parallel and one V1 PVT-MG collectors in series, with the utilization of a "dual action" thermostatic valve, showing the water volume level in the tank throughout the year.

Table 3.2.4: Table of results from the simulation of the model of Fig. 3.2.1, including two V1 PVT-SP collectors in parallel and one V1 PVT-MG collector in series with "dual action" thermostatic valve that limits the water between 50ºC and 90ºC.

heated water produced at 50-90 deg. Celsius (kg)	59.609
water refilled in the tank (kg)	57.600
water left in the tank (kg)	4.563

By using a "dual action" thermostatic valve and slightly increasing the tank's volume, the layout model of two V1 PVT-SP collectors in parallel connected with one V1 PVT-MG collector in series (2SP+1MG) presents very good results that seem also realistic. As can be seen on Fig. 3.2.4, Fig. 3.2.5 and Fig. 3.2.6, there are many days of the year with water heated at a temperature range between 50º and 90ºC, the simulations present realistic operational behavior, and the tank is refilled correctly according to the control command given.

3 SP collectors in parallel and 1 MG collector in series

In this case, the Water Supply equation block has the function "*M_refill=LT(Vol,2.5)*5500*", meaning that every time that the tank's volume level falls below 2500 liters the water supply from the main network is activated and the tank gets 5200 liters in an hour. The Thermostatic Control equation block has the function "*Ctrl_signal=gt(50,T_out)*".

Table 3.2.5: Table of values used for the simulation of the model of Fig. 3.2.1, including three V1 PVT-SP collectors in parallel and one V1 PVT-MG collector in series.

Overall Tank Volume	8,5 m^3
Minimum Fluid Volume (low level alarm)	0,1 m^3
Maximum Fluid Volume (high level alarm)	8,4 m^3
Initial Fluid Volume	7,5 m^3
Specific Heat Capacity (c_p)	4,19 KJ/kg.K
Water density	1000 kg/m^3

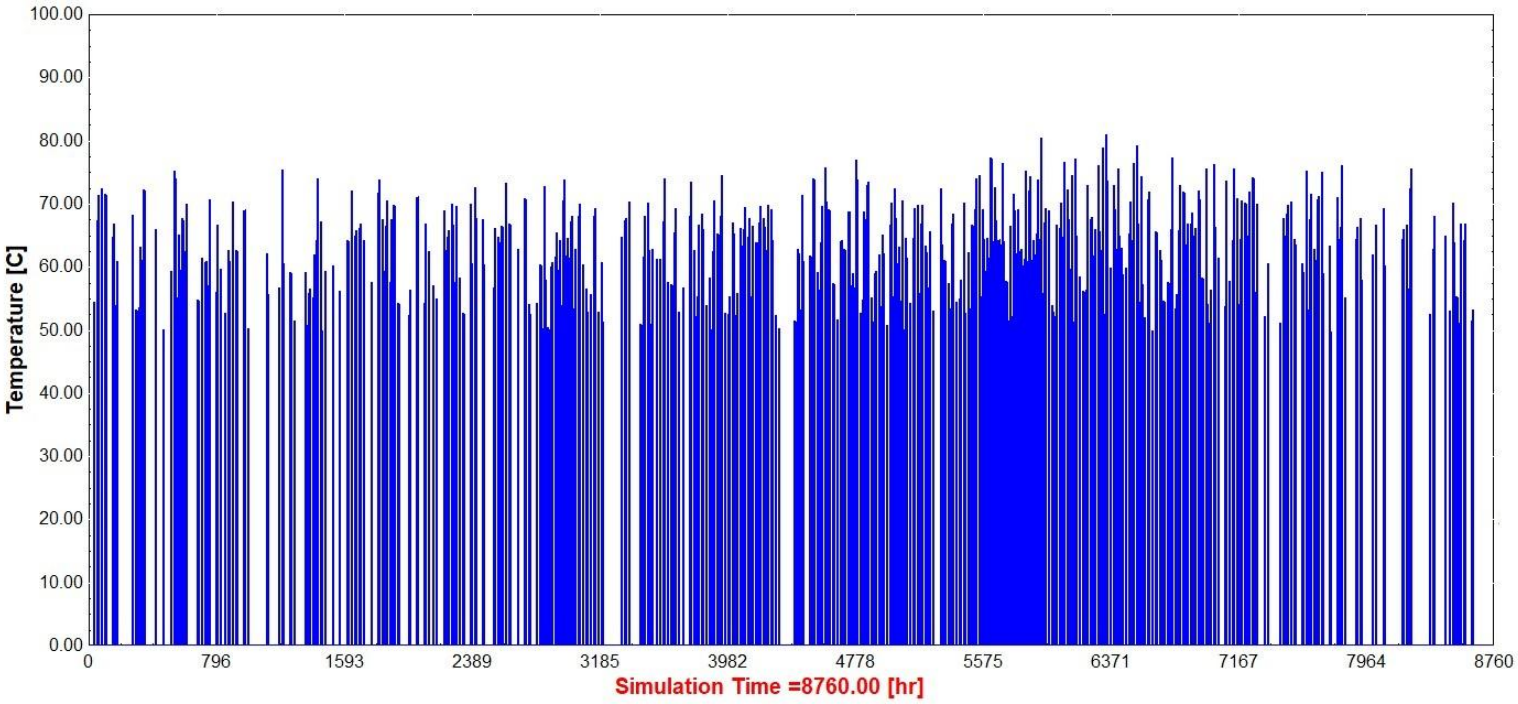

Fig. 3.2.7: Diagram (made in TRNSYS) based on simulations of the model of Fig. 3.2.1., including three V1 PVT-SP collectors in parallel and one V1 PVT-MG collectors in series, depicting the hours of the year that water flow temperature exceeds 50^{o}C and it is directed outside the closed-loop system.

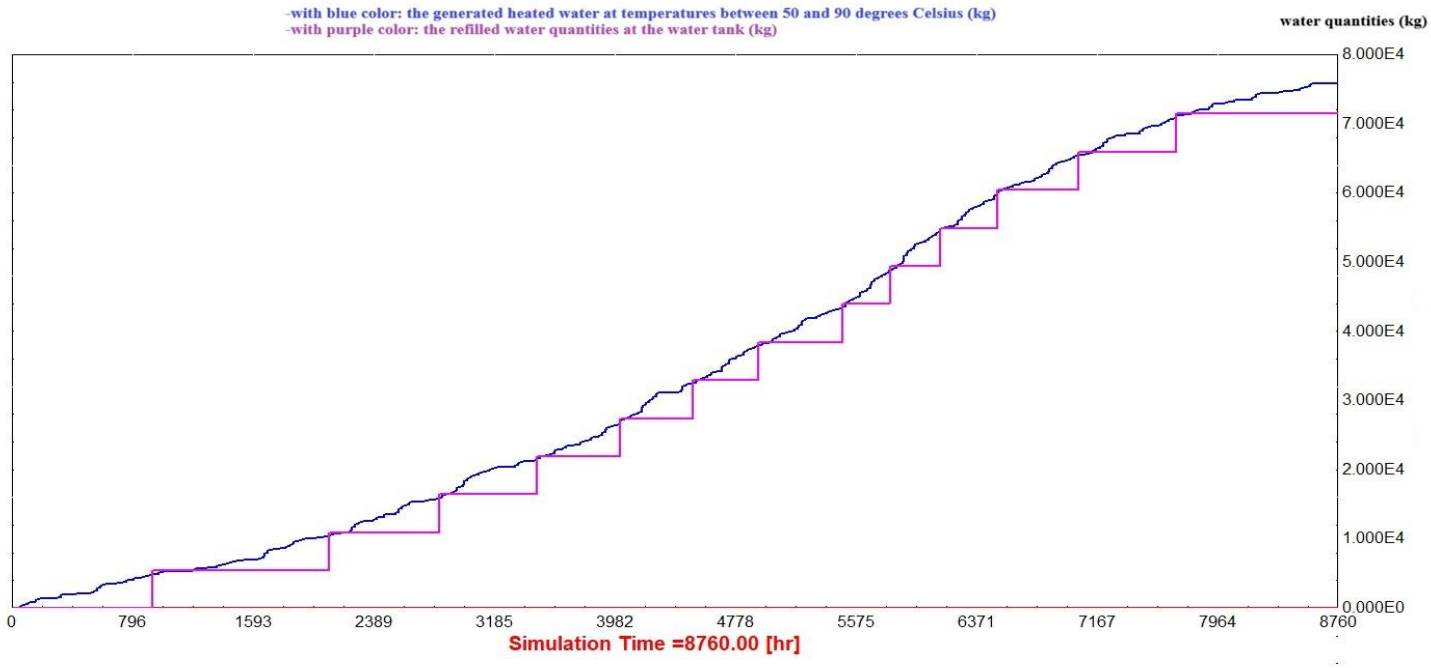

Fig. 3.2.8: Diagram (made in TRNSYS) produced by the simulations of the model of Fig.3.2.1, including three V1 PVT-SP collectors in parallel and one V1 PVT-MG collectors in series, showing the heated water generated above 50ºC as well as the refilled water quantities in the tank throughout the year

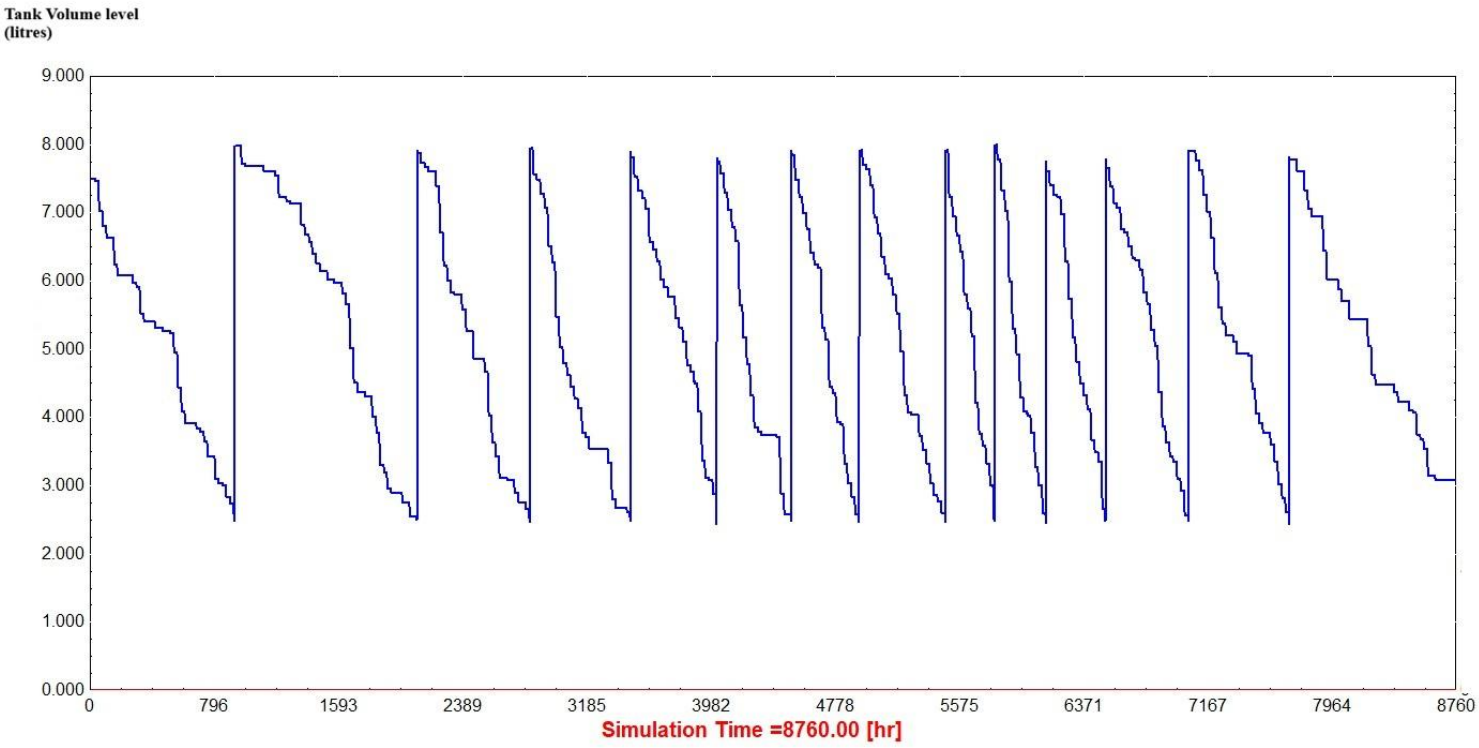

Fig. 3.2.9: Diagram (made in TRNSYS) produced by the simulations of the model 3.2.1, including three V1 PVT-SP collectors in parallel and one V1 PVT-MG collectors in series, showing the water volume level in the tank throughout the year.

As illustrated in Fig. 3.2.7, the water outlet temperature remains consistently below 90°C, thereby eliminating the need for a dual-action valve. As shown in Fig. 3.2.8 and Fig. 3.2.9, the simulations demonstrate realistic operational behavior; the tank is refilled correctly according to the programmed control command.

Table 3.2.6: Table of results from the simulation of the model of Fig. 3.2.1, including three V1 PVT-SP collectors in parallel and one V1 PVT-MG collector in series.

heated water produced at 50-90 deg. Celsius (kg)	75.913
water refilled in the tank (kg)	71.500
water left in the tank (kg)	3.087

4 SP collectors in parallel and 1 MG collector in series

In this case, the Water Supply equation block has the function "*M_refill=LT(Vol,3.5)*6500*", meaning that every time that the tank's volume level falls below 3500 liters the water supply from the main network is activated and the tank gets 6400 liters in an hour.

Table 3.2.7: Table of values used for the simulation of the model of Fig. 3.2.1, including four V1 PVT-SP collectors in parallel and one V1 PVT-MG collector in series.

Overall Tank Volume	10,5 m^3
Minimum Fluid Volume (low level alarm)	0,1 m^3
Maximum Fluid Volume (high level alarm)	10,4 m^3
Initial Fluid Volume	9,5 m^3
Specific Heat Capacity (c_p)	4,19 KJ/kg.K
Water density	1000 kg/m^3

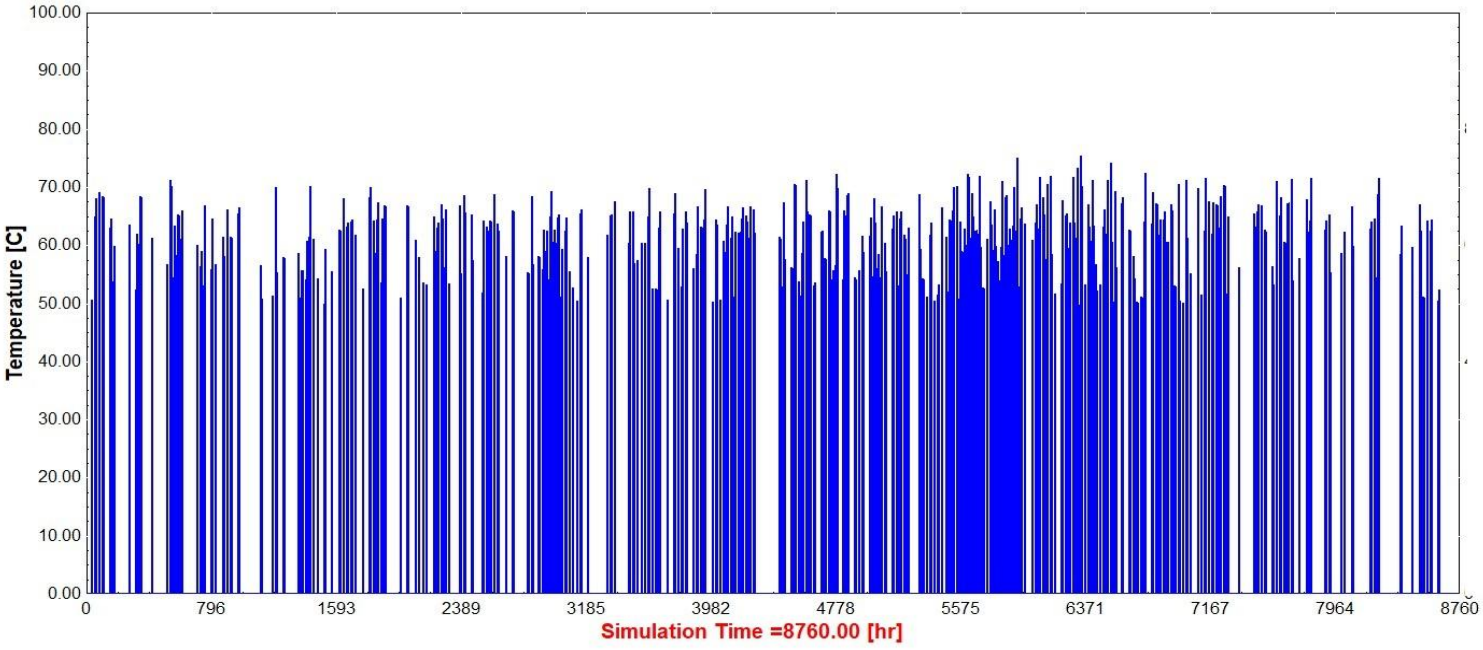

Fig. 3.2.10: Diagram (made in TRNSYS) based on simulations of the model of Fig. 3.2.1., including four V1 PVT-SP collectors in parallel and one V1 PVT-MG collectors in series, depicting the hours of the year that water flow temperature is above 50ºC and it is directed outside

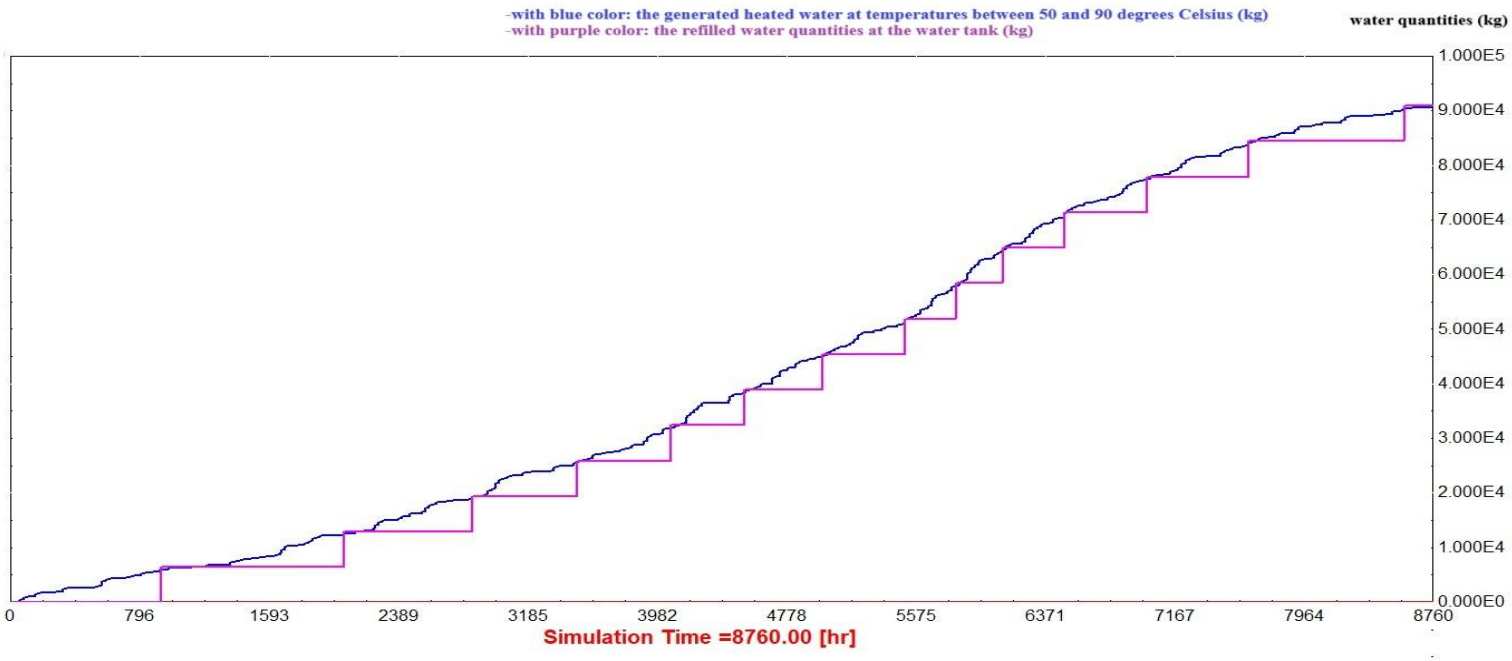

Fig. 3.2.11: Diagram (made in TRNSYS) produced by the simulations of the model of Fig.3.2.1, including four V1 PVT-SP collectors in parallel and one V1 PVT-MG collectors in series, showing the heated water generated above 50ºC as well as the refilled water quantities in the tank throughout the yearthe closed-loop system.

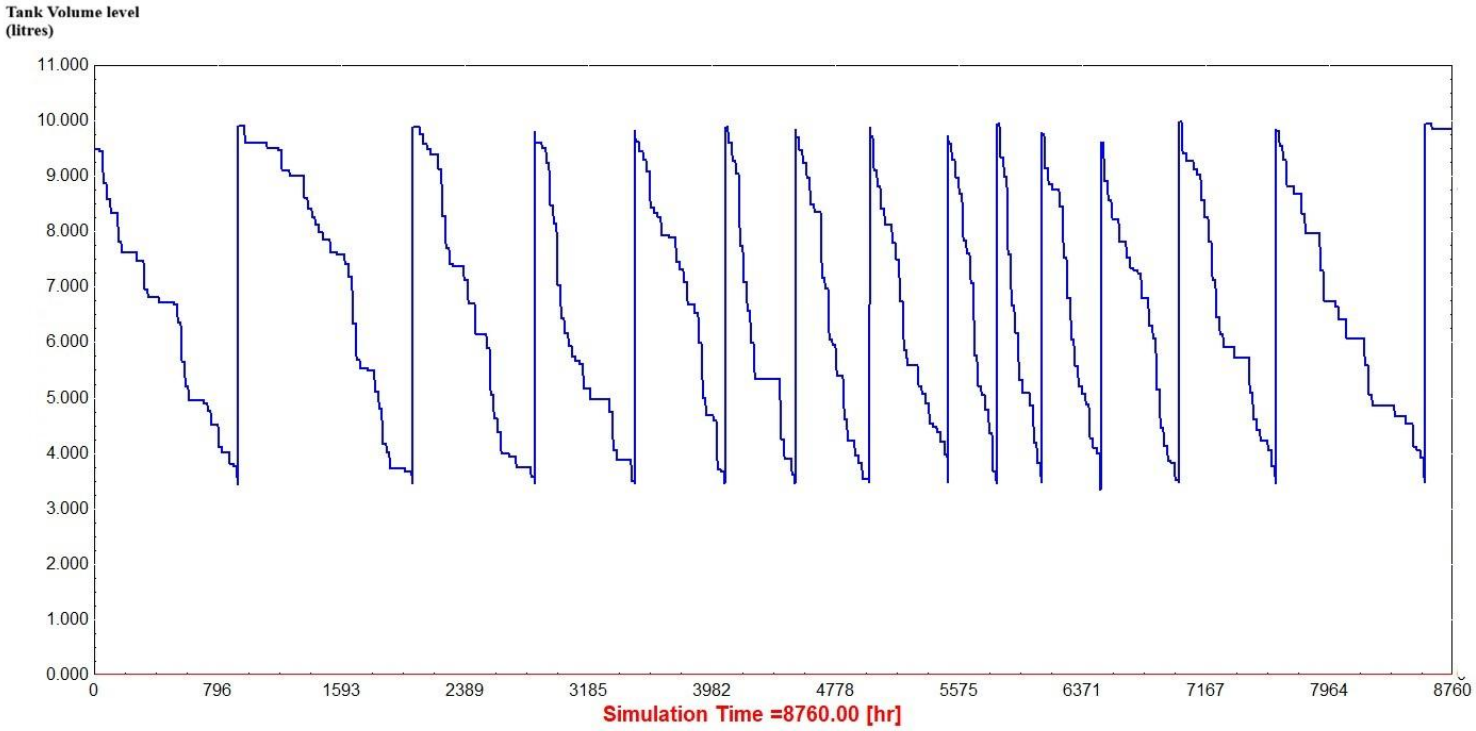

Fig. 3.2.12: Diagram (made in TRNSYS) produced by the simulations of the model in Fig. 3.2.1, including V1 PVT-SP collectors in parallel and one V1 PVT-MG collectors in series, showing the water volume level in the tank throughout the year.

As shown, in the graphs above, the model layout includes four V1 PVT-SP collectors in parallel and one V1 PVT-MG collectors in series (4SP+1MG) model layout functions appropriately giving realistic demonstrations, too, regarding water filling in the tank and heated water generation in temperatures in the range of 50º-90ºC. In this model, as well, there is no need of the "dual action" thermostatic valve and the function of the Thermostatic Control in TRNSYS is "*Ctrl_signal=gt(50,T_out)*". However, it can be observed that the water outlet temperature remains steadily below 80ºC, and this can probably lead to lower efficiency of electrolysis and thus increase of energy required for the process.

Table 3.2.8: Table of results from the simulation of the model of Fig. 3.2.1, including four V1 PVT-SP collectors in parallel and one V1 PVT-MG collector in series.

heated water produced at 50-90 deg. Celsius (kg)	90.624
water refilled in the tank (kg)	91.000
water left in the tank (kg)	9.863

3.3. Water heating for Alkaline Electrolysis (70º-90ºC)

In this case, the Thermostatic Control equation block has the function "*Ctrl_signal= and(gt(70,T_out),lt(90,T_out))*", meaning that the valve is activated when the temperature is in a range between 70ºC and 90ºC. This function practically acts as a "dual action" thermostatic valve deactivated when the water temperature is below 70 ºC and above 90ºC.

1 SP collector and 1 MG collector in series with "dual action" thermostatic valve

In this case, the Water Supply equation block has the function "*M_refill=LT(Vol,2)*3800*", meaning that every time that the tank's volume level falls below 2000 liters the water supply from the main network is activated and the tank gets 3800 liters in an hour. The tank used for this model is larger than the one utilized in the PEM electrolysis scenario, as the required temperatures are within a higher range. Consequently, a larger tank provides greater thermal management, ensuring a lower inlet temperature and preventing the thermal degradation of the collector. Furthermore, it is necessary to increase the water flow rate range to maintain the WISC collector's outlet temperature below 60°C. Therefore, various upper flow rate limits were applied incrementally to identify the optimal value that satisfies this criterion. As shown below in Table 3.3.2 and Fig. 3.3.1, for a water flowrate of 64,5 kg/hr and above, the water outlet temperature of the V1 PVT-SP collector remains below 60°C. For this reason, an upper waterflow limit of 65 kg/hr is chosen.

Table 3.3.1: Table of values used for the simulation of the model of Fig. 3.2.1, including one V1 PVT-SP collector and one V1 PVT-MG collector in series with "dual action" thermostatic valve that limits the operational temperature range between 70°C and 90°C.

Overall Tank Volume	6 m^3
Minimum Fluid Volume (low level alarm)	0,1 m^3
Maximum Fluid Volume (high level alarm)	5,9 m^3
Initial Fluid Volume	4,5 m^3
Specific Heat Capacity (c_p)	4,19 KJ/kg.K
Water density	1000 kg/m^3

Table 3.3.2: Table of values of maximum water outlet temperature of V1 PVT-SP collector for various maximum flowrate limits, for the model of Fig.3.2.1, including one V1 PVT-SP collector and 1 V1 PVT-MG collector in series with "dual action" thermostatic valve that limits the operational temperature range between 70°C and 90°C.

max flowrate limit (kg/hr)	T_max at outlet of SP collector (deg. C)
50	68,22
60	62,58
65	59,69
70	58,99

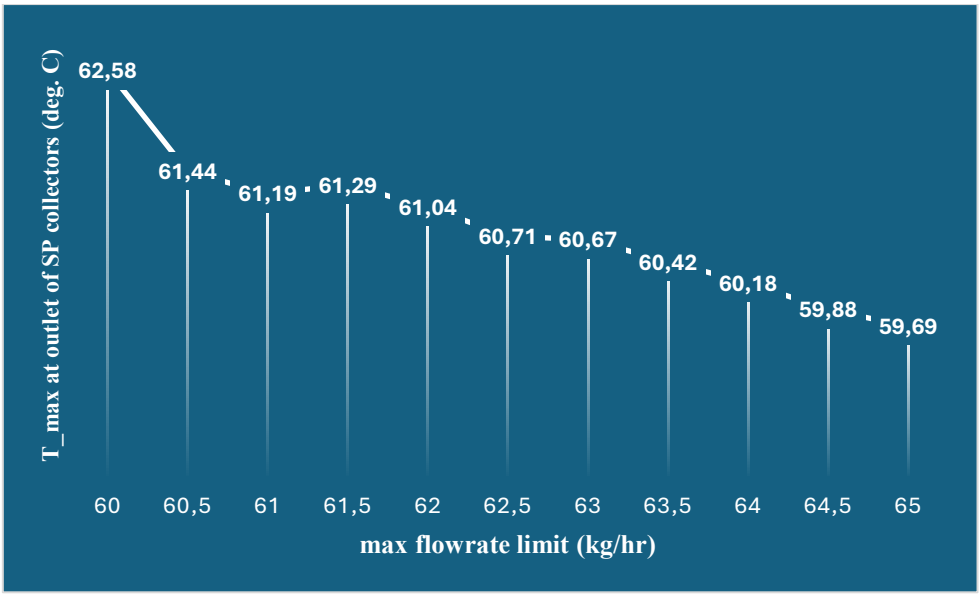

Fig. 3.3.1: Diagram of the maximum water outlet temperature of V1 PVT-SP collector for the model of Fig.3.2.1, including one V1 PVT-SP collector and one V1 PVT-MG collector in series with the utilization of a "dual action" thermostatic valve that limits the water temperature for the exit of the loop between 70ºC and 90ºC**,** based on the results of the simulations in TRNSYS.

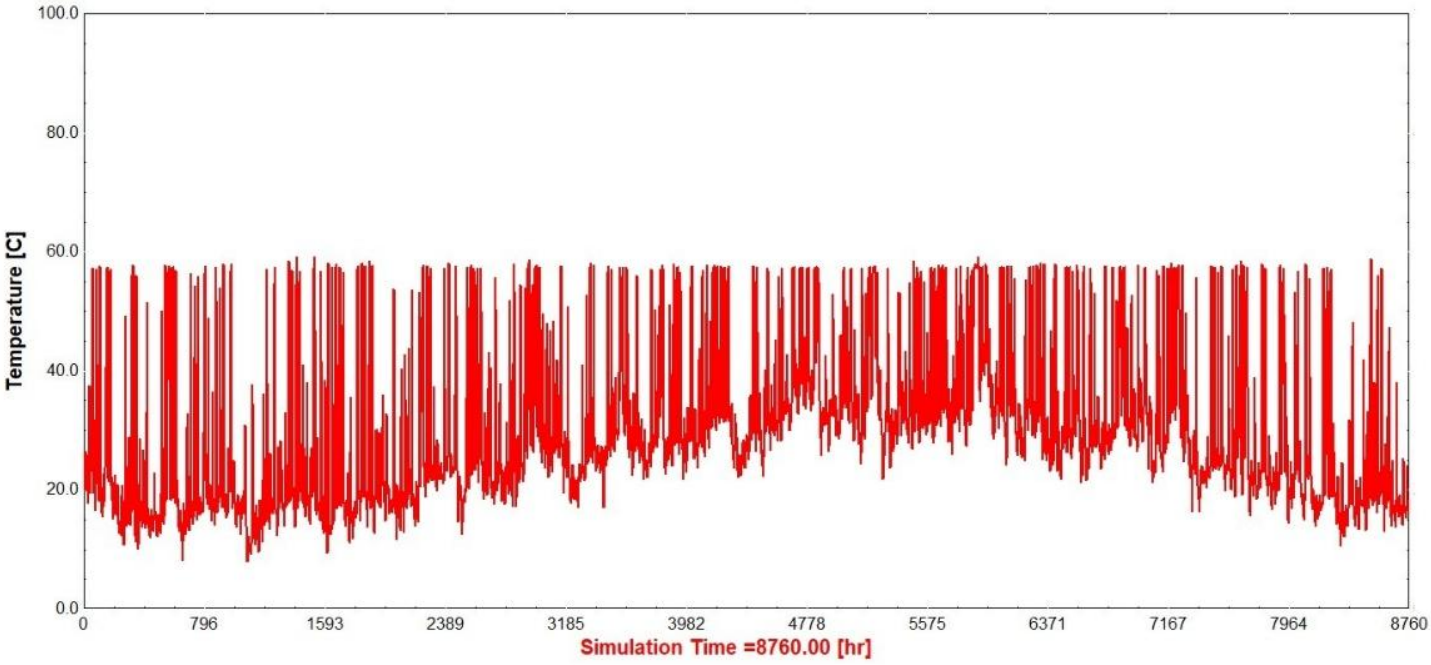

Fig. 3.3.2: Diagram (made in TRNSYS) produced by the simulations of the model of Fig. 3.2.1 (including one V1 PVT-SP collector and one V1 PVT-MG collector in series with the utilization of a "dual action" thermostatic valve that limits the water temperature for the exit of the loop between 70ºC and 90ºC) of the water outlet temperature of the V1 PVT-SP collector throughout the year in a mass flowrate range between 11,5 and 82 kg/hr and a PID control system adjusting the water flowrate in order to maintain the setpoint temperature of 57,5ºC. The outlet temperature does not exceed 60ºC throughout the year.

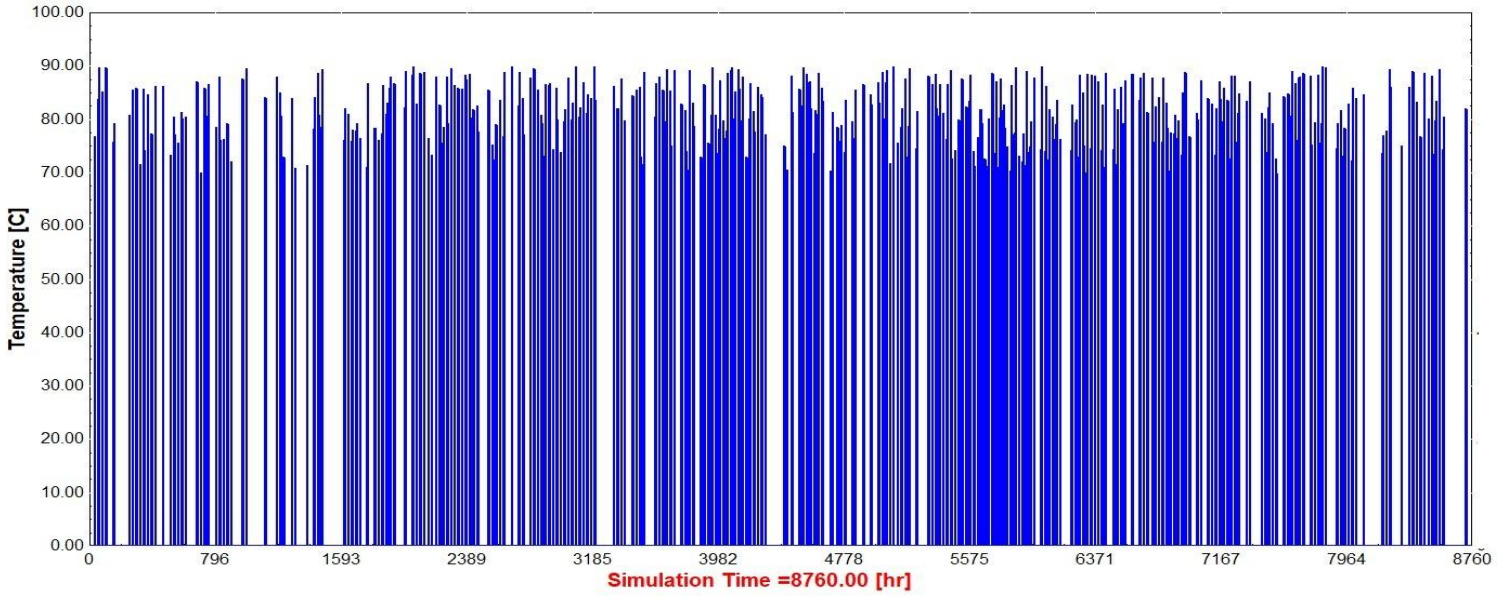

Fig. 3.3.3: Diagram (made in TRNSYS) based on simulations of the model of Fig. 3.2.1., including one V1 PVT-SP and one V1 PVT-MG collectors in series, with the utilization of a "dual action" thermostatic valve, depicting the hours of the year that water flow temperature is between 70ºC and 90ºC, and it is directed outside the closed-loop system.

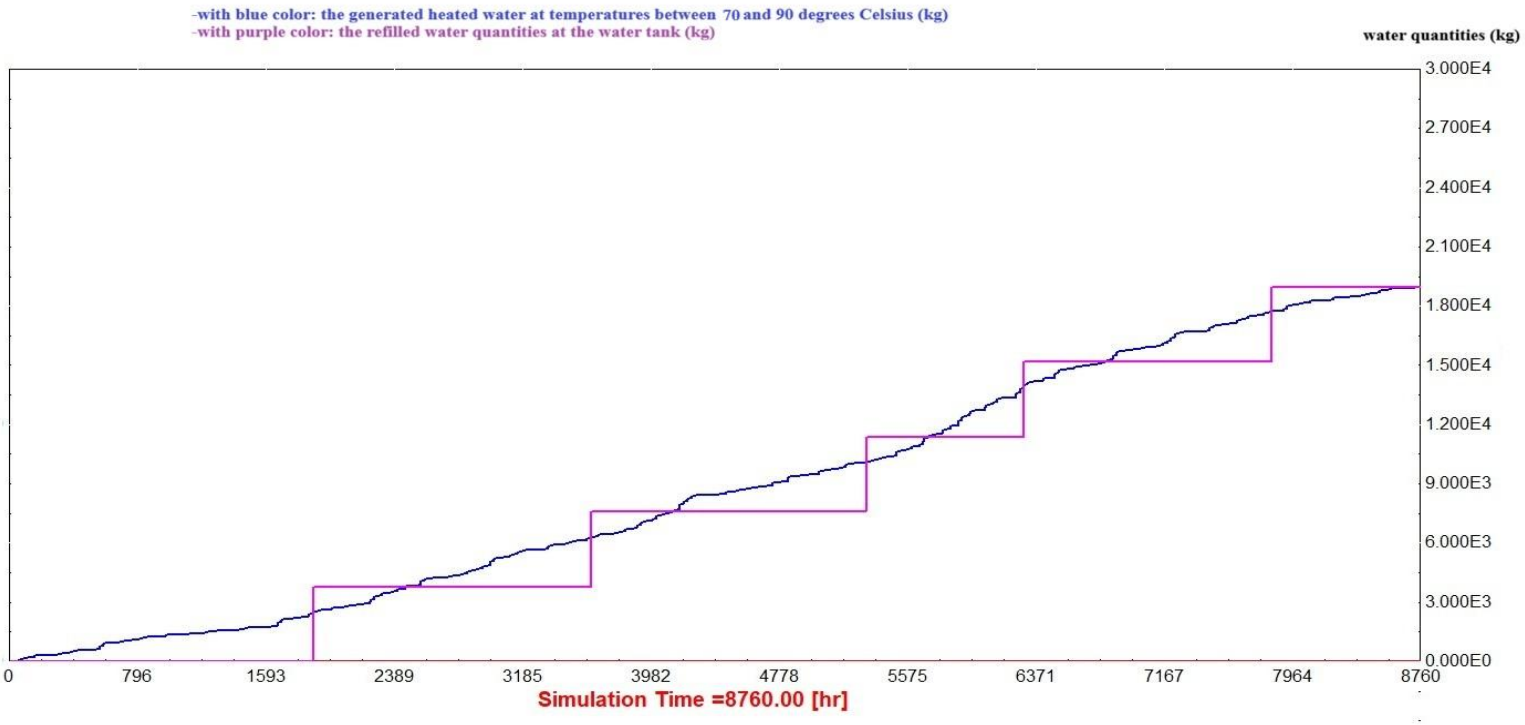

Fig. 3.3.4: Diagram (made in TRNSYS) produced by the simulations of the model of Fig.3.2.1, including two V1 PVT-SP collectors in parallel and one V1 PVT-MG collectors in series, with the utilization showing the heated water generated in an operational temperature range between 70ºC and 90ºC, as well as the refilled water quantities in the tank throughout the year

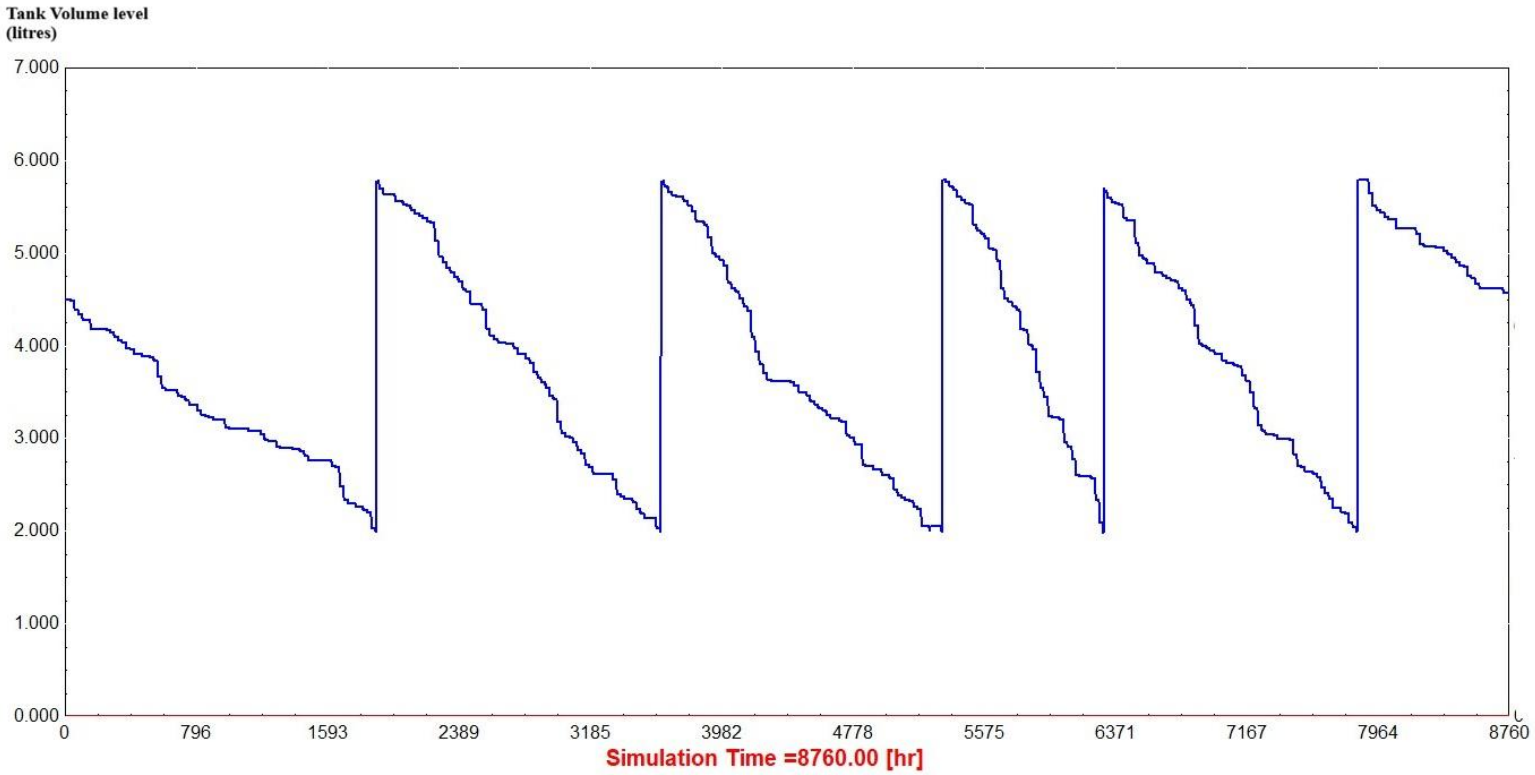

Fig. 3.3.5: Diagram (made in TRNSYS) produced by the simulations of the model in Fig. 3.2.1, including one V1 PVT-SP and one V1 PVT-MG collectors in series, with the utilization of a "dual action" thermostatic valve that limits the operational temperature range between 70°C and 90°C, showing the volume level in the tank throughout the year.

Table 3.3.3: Table of results from the simulation of a model including one V1 PVT-SP collector and one V1 PVT-MG collector in series with the utilization of a "dual action" thermostatic valve that limits the operational temperature range between 70°C and 90°C.

heated water produced at 70-90 deg. Celsius (kg)	18.978
water refilled in the tank (kg)	19.000
water left in the tank (kg)	4.577

2 SP collectors in parallel and 1 MG collector in series with "dual action" thermostatic valve

In this case, the Water Supply equation block has the function "M_refill=LT(Vol,4)*5800", meaning that every time that the tank's volume level falls below 4000 liters the water supply from the main network is activated and the tank gets 5800 liters in an hour. In this case, too, the tank used for this model is larger than the one utilized in the PEM electrolysis scenario, as the required temperatures are within a higher range. Once again, a larger tank provides greater thermal management, ensuring lower inlet temperatures and preventing the thermal degradation of the collector. Increasing the water flow rate range, to maintain the WISC collector's outlet temperature below 60°C, is crucial and various upper flow rate limits were applied to identify the optimal value that satisfies this criterion. As shown below in Fig. 3.3.6, for

a water flowrate of 155 kg/hr and above, the water outlet temperature of the V1 PVT-SP collector remains below 60°C. In this case, an upper waterflow limit of 156 kg/hr is chosen (of a flow directed at both V1 PVT-SP collectors), which corresponds to a waterflow limit of 78 kg/hr for each one of the V1 PVT-SP collectors.

Table 3.3.4: Table of values used for the simulation of the model of Fig. 3.2.1, including two V1 PVT-SP collectors connected in parallel and one V1 PVT-MG collector in series with "dual action" thermostatic valve that limits the operational temperature range between 70°C and 90°C.

Overall Tank Volume	10 m^3
Minimum Fluid Volume (low level alarm)	0,1 m^3
Maximum Fluid Volume (high level alarm)	9,9 m^3
Initial Fluid Volume	8,5 m^3
Specific Heat Capacity (c_p)	4,19 KJ/kg.K
Water density	1000 kg/m^3

Table 3.3.5: Table of values of maximum water outlet temperature of V1 PVT-SP collector for various maximum flowrate limits, for the model of Fig.3.2.1, including two V1 PVT-SP collectors connected in parallel and one V1 PVT-MG collector in series with "dual action" thermostatic valve that limits the operational temperature range between 70°C and 90°C.

max flowrate limit (kg/hr)	T_max at outlet of SP collector (deg. C)
150	61,16
155	59,81
160	59,54

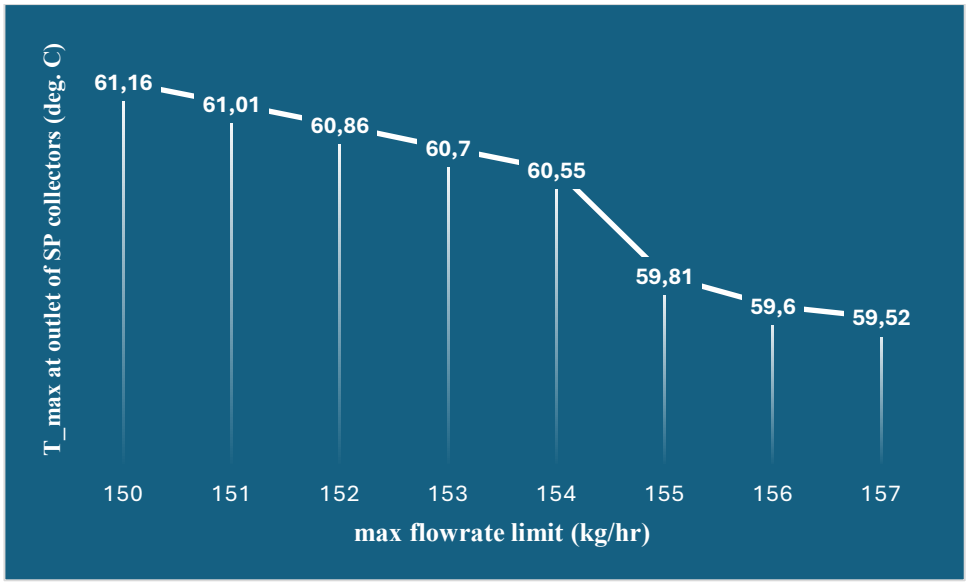

Fig. 3.3.6: Diagram of the maximum water outlet temperature of V1 PVT-SP collector for the model of Fig.3.2.1, including two V1 PVT-SP collectors connected in parallel and one V1 PVT-MG collector in series with the utilization of a "dual action" thermostatic valve that limits the water temperature for the exit of the loop between 70ºC and 90ºC**,** based on the results of the simulations in TRNSYS.

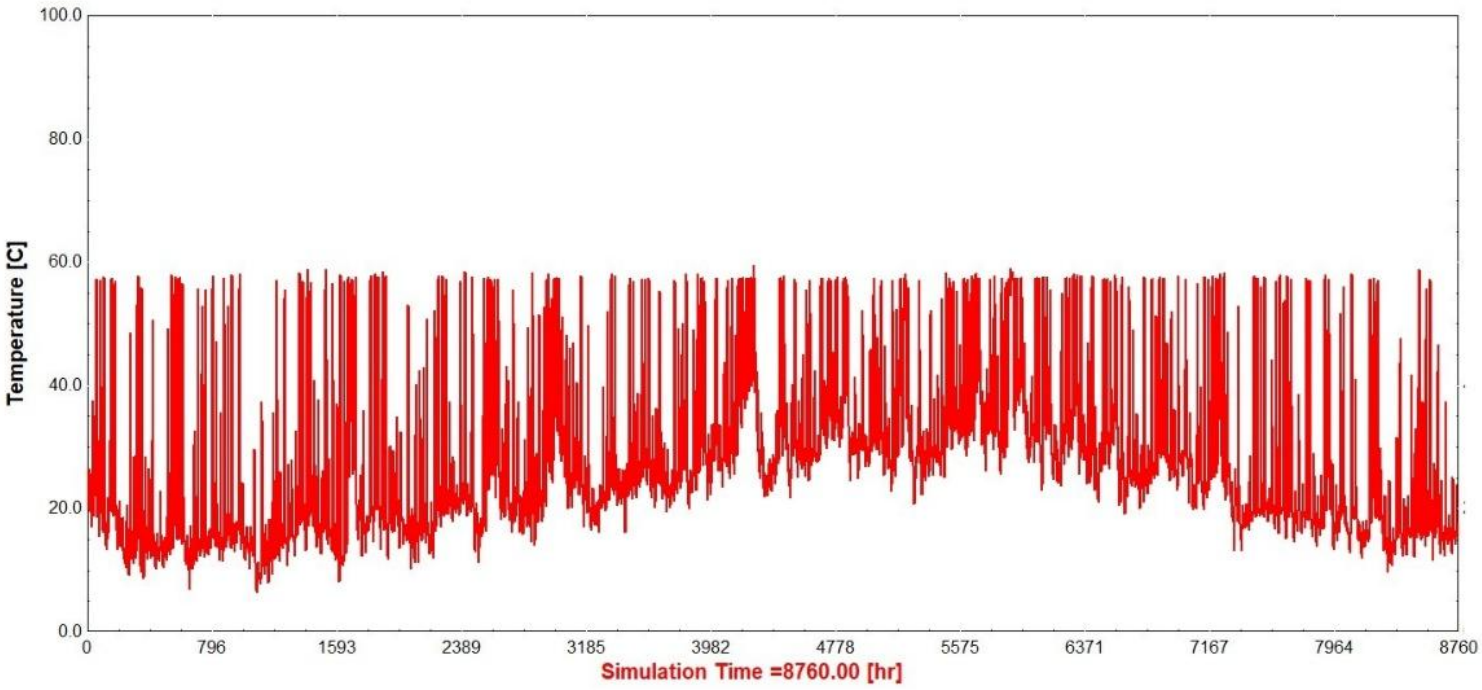

Fig. 3.3.7: Diagram (made in TRNSYS) produced by the simulations of the model of Fig. 3.2.1 (including two V1 PVT-SP collectors connected in parallel and one V1 PVT-MG collector in series with the utilization of a "dual action" thermostatic valve that limits the water temperature for the exit of the loop between 70ºC and 90ºC) of the water outlet temperature of the V1 PVT-SP collector throughout the year in a mass flowrate range between 11,5 and 178 kg/hr and a PID control system adjusting the water flowrate in order to maintain the setpoint temperature of 57,5ºC. The outlet temperature does not exceed 60ºC throughout the year.

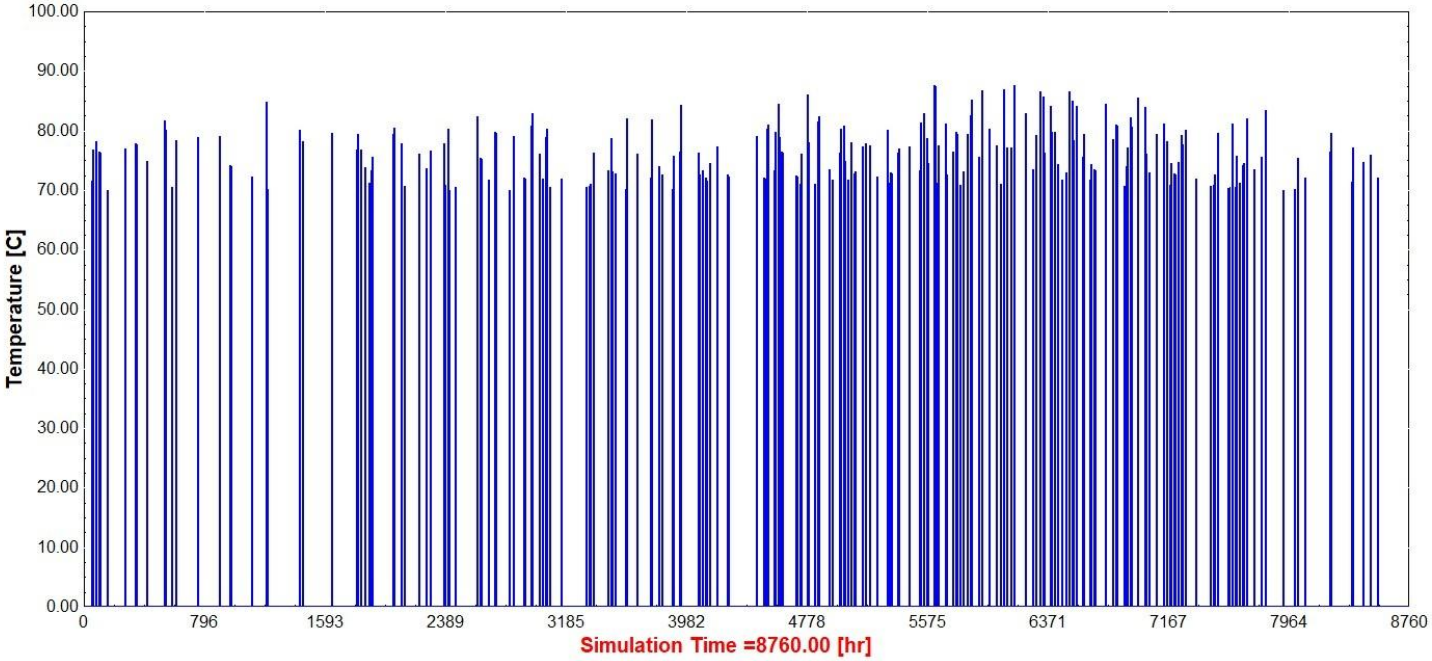

Fig. 3.3.8: Diagram (made in TRNSYS) based on simulations of the model of Fig. 3.2.1., including two V1 PVT-SP collectors connected in parallel and one V1 PVT-MG collectors in series, with the utilization of a "dual action" thermostatic valve, depicting the hours of the year that water flow temperature is between 70ºC and 90ºC.

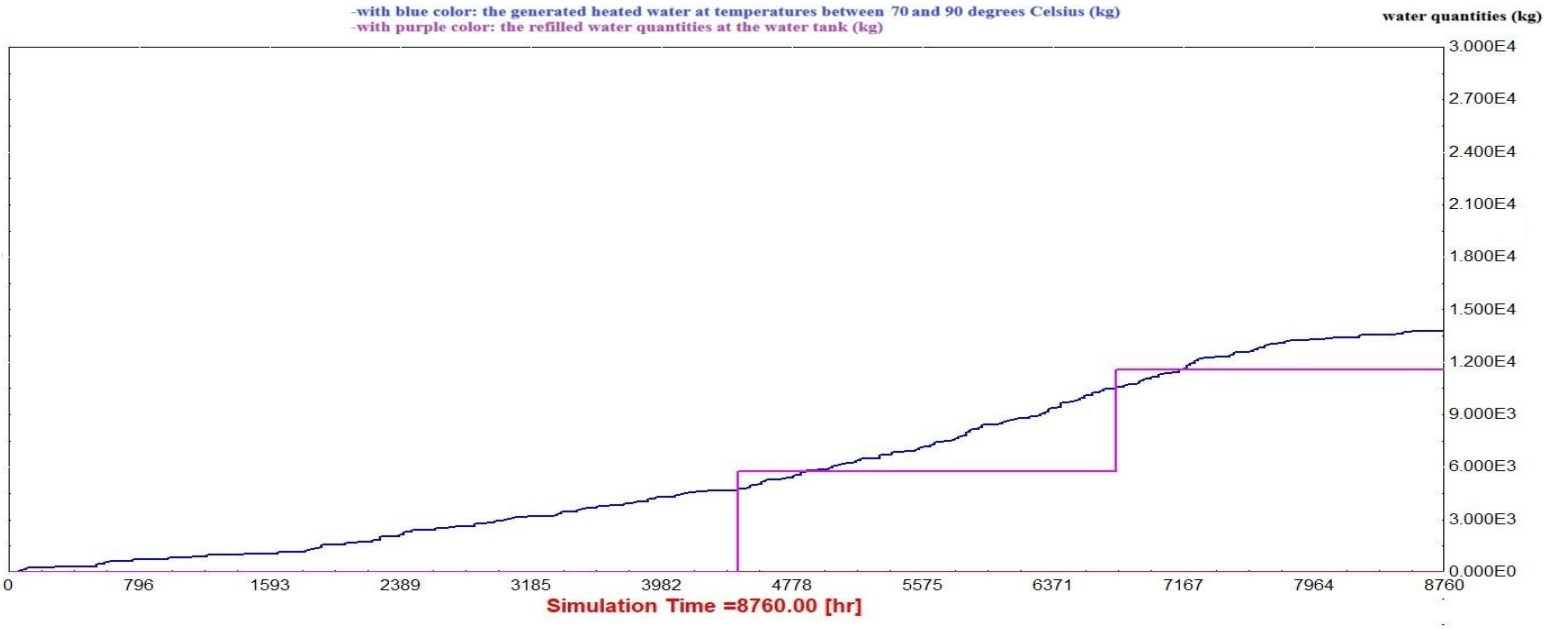

Fig. 3.3.9: Diagram (made in TRNSYS) produced by the simulations of the model in Fig. 3.2.1, including two V1 PVT-SP and one V1 PVT-MG collectors in series, with the utilization of a "dual action" thermostatic valve that limits the operational temperature range between 70ºC and 90ºC, showing the volume level in the tank throughout the year. and it is directed outside the closed-loop system.

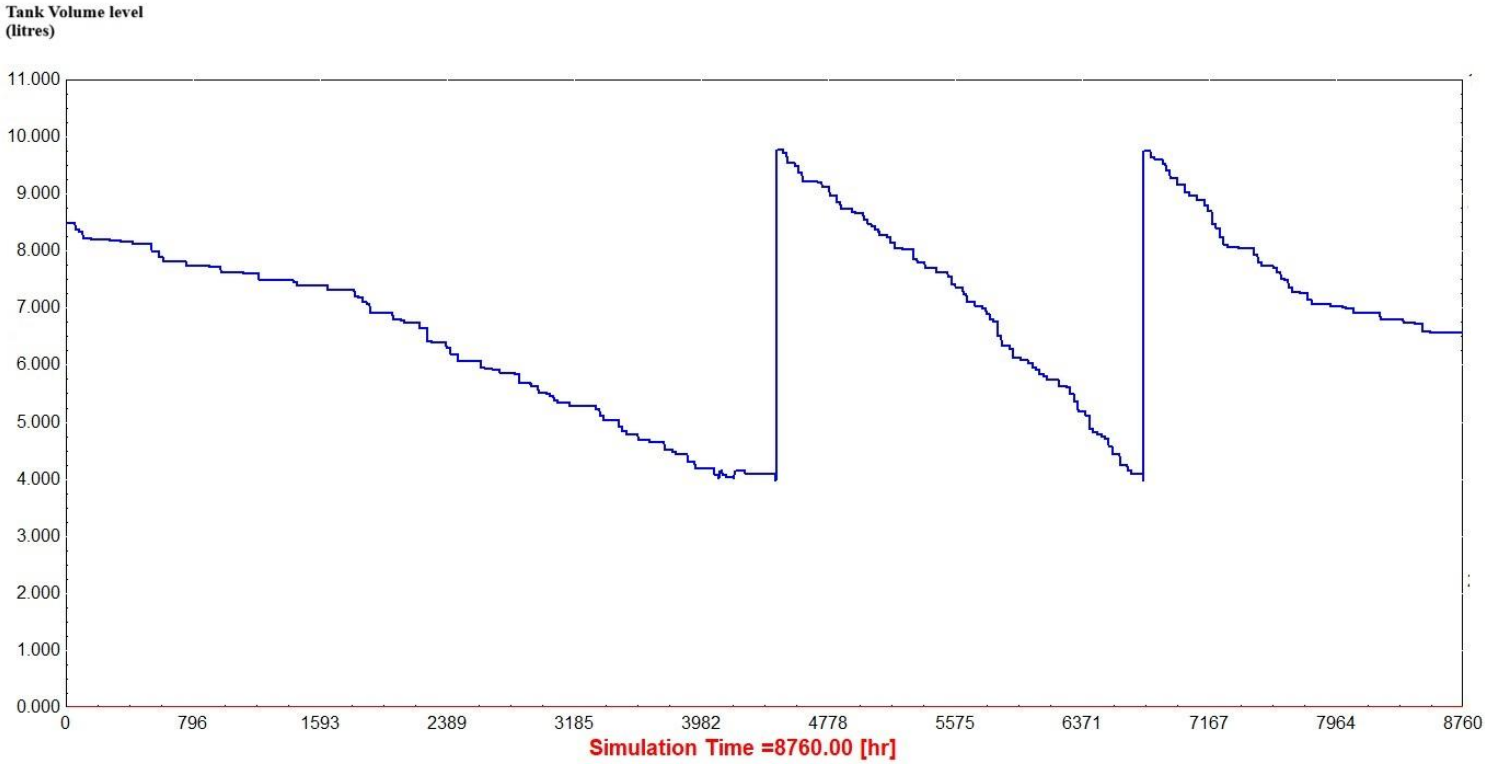

Fig. 3.3.10: Diagram (made in TRNSYS) produced by the simulations of the model in Fig. 3.2.1, including two V1 PVT-SP collectors connected in parallel and one V1 PVT-MG collectors in series, with the utilization of a "dual action" thermostatic valve that limits the operational temperature range between 70ºC and 90ºC, showing the volume level in the tank throughout the year.

Table 3.3.6: Table of results from the simulation of a model including two V1 PVT-SP collectors in parallel and one V1 PVT-MG collector in series with thermostatic valve that does not permit the water to surpass the limit of 90ºC.

heated water produced at 70-90 deg. Celsius (kg)	13.786
water refilled in the tank (kg)	11.600
water left in the tank (kg)	6.598

As shown at the graphs above, the developed layouts appear less efficient for alkaline electrolysis due to its more restricted operating temperature range compared to the PEM type. The total hours of the year during which water is heated to the required operational range are significantly fewer; furthermore, extensive dimensions of water tanks are required, too, relatively to the other two electrolysis methods. Even with the use of "dual action" thermostatic valve in order to limit up the operational temperature range, the water demands are way higher than those of the AEM and PEM methods. Consequently, a layout with three V1 PVT-SP collectors in parallel and one V1 PVT-MG collector in series is not only an inefficient option but may also increase the required water flow rates beyond the operational limits of the MG collector. Moreover, the immense ranges between the lowest and the highest water flowrate limits make the implementation of variable-speed pumps a less applicable scenario.

4. Results & Discussion

4.1. Baseline Collectors' Allocation and Layout Results

Table 4.1.1: Table with definitions of the minimum number of collectors each model layout needs to achieve at appropriate temperatures the heating of 123.000.000 kgs of water per year and thus can achieve a reduction by 10% of the CO_2 emissions of the industry.

Layout models	number of SP collectors needed	number of MG collectors needed
1 SP collector's model for AEM electrolysis	6168	-
2 SP + 1 MG collectors' model for PEM electrolysis (with "dual action" thermostatic v/v)	4142	2071
3 SP +1 MG collectors' model for PEM electrolysis	4863	1621
4 SP +1 MG collectors' model for PEM electrolysis	5432	1358
1 SP +1 MG collectors' model for alkaline electrolysis. (with "dual action" thermostatic v/v)	6730	6730
2 SP +1 MG collectors' model for alkaline electrolysis. (with "dual action" thermostatic v/v)	17838	8919

It is evident that alkaline electrolysis is not the most suitable choice for this specific case due to its temperature limitations, which is a constraint that the existing infrastructure, available collector types and local climate data cannot easily support and require greater infrastructure and thus much more resources. Meanwhile, the greater range between the low and the upper limits of the water flowrate makes the implementation of variable speed pumps much more challenging. Furthermore, the excessive water resource requirements in comparison to other electrolysis methods render the alkaline method less favorable.

In contrast, anion exchange membrane (AEM) electrolysis appears to be the optimal choice regarding thermodynamics and resource utilization. For these specific requirements, the use of WISC collectors alone may be sufficient, making the process more straightforward and cost-effective. Furthermore, this application saves valuable facility space; the lower required temperature range is more easily achieved with fewer collectors, allowing each unit to process greater quantities of water compared to other methods. However, its early stage of development may render it premature for immediate implementation, potentially leading to significantly higher installation and operational costs.

PEM (proton exchange membrane) electrolysis is the most commercialized option and offers a relatively broad range of operating temperatures. While it requires fewer WISC collectors, it also necessitates the use of parabolic collectors to achieve the higher temperature ranges required to enhance efficiency. All three layouts offer distinct advantages, and the final selection must account for several variables. The 2SP+1MG layout provides the highest thermodynamic efficiency; however, while it minimizes the

number of WISC collectors, it requires the highest number of parabolic collectors. The 4SP+1MG layout offers a more economical alternative, though at the expense of thermodynamic efficiency, as temperature levels are significantly lower. Moreover, something crucial for the project is the definition of the electricity needs to carry out each type of electrolysis, since a part of the electricity generated in the PV solar park can be used for this reason. Ultimately, factors such as available space, economic constraints, and water resources must be thoroughly assessed to determine the most viable configuration.

4.2. Boundary Parameter Sensitivity Analyses

To evaluate the stability of the previously developed layouts, two separate sensitivity analyses were performed. In the first analysis, the network freshwater supply temperature varied by decreasing and then increasing it by 2°C compared to the baseline values utilized in the simulation models in Chapter 3. In the second analysis, the total solar irradiance varied by 5% against the baseline configuration. To implement this parameter, shift accurately, the individual components (beam radiation on the tilted surface, sky diffuse radiation and ground diffuse radiation) were scaled proportionally by the same percentage bounds.

The modifications mentioned above were applied to TRNSYS, through which the results of both analyses are extracted. Many practical reasons justify the necessity of these sensitivity analyses, including the long-term impacts of climate change on the island, the frequent dust storms characteristic of the Eastern Mediterranean region, as well as the 24-kilometer distance between the Vassiliko PV park and the Larnaca meteorological station (Lazoglou et al., 2024), (Achilleos et al., 2020). Collectively, these real-world environmental and geographical factors can introduce significant deviations into the baseline data, directly affecting system performance. The model layouts configured for the alkaline electrolysis temperature range are excluded from the following sensitivity analyses, because as demonstrated in the previous section, alkaline electrolysis proves to be the least suitable method for this specific project due to its stringent thermal and operational constraints.

Table 4.2.1: Table presenting the analysis of sensitivity made, based on changing the temperature of feeding water compared to the values used before (-2/+2ºC) and taking results by using TRNSYS. At the right part, it can be seen how much (as a percentage) the generation of heated water at the required temperature range is impacted (decreased or increased) compared with the target of generating 123.000.000 kgs of heated water per year.

Layout models	Water Temperature difference (ºC)	Percentage deviation of the target (%)
1 SP collector's model for AEM electrolysis	-2/+2	-1,93/+1,66
2 SP +1 MG collectors' model for PEM electrolysis (with "dual action" thermostatic v/v)	-2/+2	-0,61/+0,05
3 SP +1 MG collectors' model for PEM electrolysis	-2/+2	-0,56/+1,19
4 SP +1 MG collectors' model for PEM electrolysis	-2/+2	-1,18/+1,23

Table 4.2.2: Table presenting the analysis of sensitivity made, based on changing the total irradiance compared to the values used before (-5/+5%) and taking results by using TRNSYS. At the right part, it can be seen how much (as a percentage) the generation of heated water at the required temperature range is impacted (decreased or increased) compared with the target of generating 123.000.000 kgs of heated water per year.

Layout models	Total irradiance difference	Percentage deviation of the target (%)
1 SP collector's model for AEM electrolysis	-5%/+5%	-6,96/+5,55
2 SP +1 MG collectors' model for PEM electrolysis (with "dual action" thermostatic v/v)	-5%/+5%	-6,39/+4,35
3 SP +1 MG collectors' model for PEM electrolysis	-5%/+5%	-6,84/+7,00
4 SP +1 MG collectors' model for PEM electrolysis	-5%/+5%	-7,64/+7,38

When modifying the freshwater supply temperature, the simulation models configured for the PEM electrolysis method present an obviously lower sensitivity to temperature changes than the model developed for the AEM electrolysis method. Specifically, the 2SP+1MG layout demonstrates the smallest output variance across the temperature shifts, something that makes this architectural choice as the most thermodynamically resilient configuration for the given scenario. In the case of variations in total solar irradiance, both the PEM and AEM models display noticeable deviations in annual heated water quantities. The 2SP+1MG layout once again presents the smallest operational variance, even though its sensitivity to environmental irradiance fluctuations remains substantial.

4.3. Constraints and future work recommendations

As previously shown, the PEM model layouts exhibit the widest operational temperature range. This flexibility, combined with their mature commercialization, makes them highly adaptable to a variety of industrial applications. Compared to the AEM model framework, the PEM configurations provide superior stability under freshwater supply temperature fluctuations; something that does not equally happen on the case of total irradiance sensitivity analysis. Consequently, if climatic fluctuations remain narrow, resource availability is constrained, and the emerging AEM technology reaches commercial maturity, the AEM layout could serve as a highly viable scenario. Nevertheless, under real-world operating conditions, the PEM method remains the most practical and readily applicable option. Within the PEM configurations, the 2SP+1MG layout demands significantly more capital and material resources than the other two configurations; yet it delivers much better thermodynamic efficiency and a slightly more resilient response to ambient environmental shifts. Ultimately, the selection of the optimal configuration requires a multi-criteria compromise that accounts for the diverse variables detailed below. While this project's constraints vary, they can be further evaluated in future research. Key technical considerations for future assessment include:

- Control Systems: In this thesis, PID control was utilized within the TRNSYS software as a "black box." In a practical application, it will be necessary to select a physical PID control system that matches or exceeds the performance of the simulated model.
- Thermal Protection: A detection system must be implemented to ensure the water inlet temperature consistently remains below the surface temperature of the collectors. This is vital to minimize the thermal decay of both the PV panels and the solar thermal collectors.
- Thermal loss coefficients: In this thesis, the thermal loss coefficients of pipes and tanks are considered negligible. In real life, the materials used for the creation of a project like this define the values of these coefficients. Thus, a future analysis should be evaluated regarding that.
- Pump Selection: The selection of pumps is a critical step. The layout models utilize variable speed pumps to maintain high thermodynamic efficiency and optimize thermal energy extraction. Consequently, it is significant to prudently select the number of pumps, their capacity and their control systems based on market availability. These pumps must reliably manage the thermodynamic loads analyzed in this work, ensuring appropriate flow rates while maintaining the lowest possible electricity consumption to ensure the project remains economically and environmentally beneficial.
- Heated water accumulator: Excess heated water (meaning, quantities produced beyond immediate processing capacity) must be stored in an accumulator to preserve its thermal energy for use during periods of insufficient thermally utilizable flow. Therefore, a detailed study regarding the design and integration of such an accumulator is necessary to guarantee the system's continuous operation.
- Infrastructure and Spatial Planning: The space required for each electrolysis type, collector layout, and additional infrastructure (such as water storage tanks) must be assessed against industrial capacities and the existing layout of the PV park. Moreover, the available and commercialized carbon capture systems (CCS) must be evaluated and define which type is the most suitable and beneficial for the development of a project like this.
- Financial Constraints: Ultimately, the available financial resources invested in the project will be the determining factor in defining the scale, location and methodology of the application.

It must be stated that a project of this nature functions most effectively as part of a broader environmentally sustainable production plan and a circular economy within a specific geographical region. This integrated approach ensures the minimization of resource waste while maximizing utilization of the available resources. The generation of hydrogen for e-fuel production requires—as established above—significant quantities of water. Cyprus is an arid island that fulfills most of its water requirements through desalination plants (Xevgenos et al., 2021). Inevitably, supplying the thousands of tons of water needed for this project, desalination is an absolute necessity. Currently, the electricity mix in the Republic of Cyprus is predominantly based on fossil fuels. Therefore, a critical question for the future of this project is the carbon intensity of the energy used in the desalination process. It is essential to determine whether this energy can be derived primarily from sustainable sources or from conventional fossil fuels. In the first case, the entire methanol production chain could probably be classified as truly sustainable and environmentally friendly. In the second case, the environmental

sustainability of the methanol produced becomes highly questionable, as the emissions from water processing may offset the benefits of the e-fuel. Moreover, it can be noted that a techno-economic compromise must be acknowledged in future research. While lower thermal needs can minimize the required solar array footprints, they introduce, too, decreased electrochemical potential. An optimized project must balance the capital costs against electrical efficiency challenges within the electrolysis stack.

Another question that arises is whether a solar thermal water heating stage might be more suitable for alternative applications. Specifically, similar systems are frequently employed for district heating or as industrial pre-heating stages (Dannemand et al., 2025), (Oliveira & Iten, 2022). Consequently, future research could include a comparative evaluation to determine if these alternative applications would yield greater economic or environmental benefits than the current electrolysis-focused model. If e-fuel production is determined to be the most viable option, the feasibility of modifying the existing vehicle fleet in Cyprus to utilize methanol-gasoline blends must also be evaluated. Such a transition would not only reduce the island's reliance on fuel imports but also increase the energy independence of the island, whereas it would significantly lower the "well-to-tank" emissions associated with the decrease in the international transportation of conventional fuels to the island.

5. Conclusions

This thesis investigated the technical thermodynamic feasibility of utilizing solar thermal energy facility layouts designed to generate heated water for low-temperature industrial electrolysis aiming for e-fuel production. Driven by the target of reducing local industrial CO_2 emissions by 10% (100.000 tons), approximately 123.000 tons of heated water must be processed annually. Thermo-hydraulic simulations developed in TRNSYS evaluated different arrangements of WISC and CPC units to achieve the required inlet fluid thresholds across Anion Exchange Membrane (AEM), Proton Exchange Membrane (PEM) and alkaline electrolysis systems.

The simulation and sensitivity analyses gave several important insights regarding layout optimization results:

- **Alkaline Electrolysis:** Alkaline systems (70ºC-90ºC) proved to be the least practical option due to narrow operational temperature ranges, excessive water demands, large storage volume requirements and a high sensitivity to flow rates that complicates the system integration of variable-speed pumps.
- **AEM Electrolysis:** Anion Exchange Membrane system (40ºC-60ºC) represents the best space-efficient solution, requiring only 6.168 retrofitted WISC collectors within the existing 8 MWp solar park infrastructure, since the low temperature operational range of the electrolysis method can be satisfied only with the utilization of WISC units. However, its premature commercialization stage and high sensitivity in environmental changes present significant barriers to a probable execution in the near future.
- **PEM Electrolysis:** Proton Exchange Membrane electrolysis (50ºC-90ºC) emerges as the most stable and mature choice for real-world applications. By simulating models for this type of electrolysis, the “2SP + 1MG” layout configuration achieves the highest thermodynamic efficiency and demonstrates the greatest resilience during water supply temperature and solar irradiance fluctuations.

Eventually, this study bridges a distinct literature gap by proving that recovered solar thermal energy can supply significant thermal loads at a process of low-temperature electrolysis. While the simulation models can present a viable and efficient thermodynamic system, transitioning this system into reality needs to meet various criteria and compromises. Future work must evaluate the environmental constraints of Cyprus (such as freshwater shortage and a probable carbon footprint of seawater desalination) against spatial and regional planning limitations, real-life PID loop tuning, as well as capital and operational expenditures in order to ensure true ecological and financial sustainability and viability

6. References

Achilleos, S., Mouzourides, P., Kalivitis, N., Katra, I., Kloog, I., Kouis, P., Podas, T., Panayiotou, A., Agathangelou, V., Savvides, C. and Koutrakis, P., 2020. Spatio-temporal variability of desert dust storms in Eastern Mediterranean (Crete, Cyprus, Israel) between 2006 and 2017 using a uniform methodology. *Science of the Total Environment*, 714, p. 136693.

Ahmed, Y.E., Maghami, M.R., Pasupuleti, J., Danook, S.H. and Basim Ismail, F., 2024. Overview of recent solar photovoltaic cooling system approach. *Technologies*, 12(9), p. 171.

Al-Ghezi, M.K., Ahmed, R.T. and Chaichan, M.T., 2022. The Influence of Temperature and Irradiance on Performance of the photovoltaic panel in the Middle of Iraq. *International Journal of Renewable Energy Development*, 11(2), p. 501.

Ballif, C., Haug, F.J., Boccard, M., Verlinden, P.J. and Hahn, G., 2022. Status and perspectives of crystalline silicon photovoltaics in research and industry. *Nature Reviews Materials*, 7(8), pp. 597-616.

Castro Oliveira, M. and Iten, M., 2021. Modelling of A Solar Thermal Energy System for Energy Efficiency Improvement in a Ceramic Plant. *Renewable Energy and Environmental Sustainability*, 6, p. 31.

Corti, H.R., 2022. Polymer electrolytes for low and high temperature PEM electrolyzers. *Current Opinion in Electrochemistry*, 36, p. 101109.

Cyprus Energy Regulatory Authority (CERA), 2019. *Cyprus national report 2024: Monitoring report to the European Commission*. Council of European Energy Regulators. Available at: https://www.ceer.eu/wp-content/uploads/2024/04/C19_NR_Cyprus_EN.pdf.

Dalena, F., Senatore, A., Marino, A., Gordano, A., Basile, M. and Basile, A., 2018. Methanol production and applications: an overview. *Methanol*, pp. 3-28.

Dannemand, M., Furbo, S., Kong, W., Cardoso, J.P., Fação, J., Vilke, G. and Garcia, A.C., 2025. *D5.2 report on system performance of the selected PVT applications (Work Package 5, PVT4EU system integration technologies, including heat pumps and absorption chillers)*. PVT4EU – Photovoltaic and Thermal for Europe.

Eurostat, 2025a. *Household electricity prices in the EU stable in 2024*. Available at: https://ec.europa.eu/eurostat/web/products-eurostat-news/w/ddn-20250506-2.

Eurostat, 2025b. *Shedding light on energy in Europe – 2025 edition*. Available at: https://ec.europa.eu/eurostat/web/interactive-publications/energy-2025.

Google, 2026a. *Amalas, Vassiliko, Cyprus, 34°46'43.2"N 33°21'54.9"E*. Google Maps. Available at: https://www.google.com/maps/place/Amala/@34.7786765,33.3652368,1219m/data=!3m1!1e3!4m6!3m5!1s0x14e0bc72c84b2cd9:0xe4f673018c670345!8m2!3d34.7916667!4d33.3583333!16s%2Fg%2F11clw2t0qx?entry=ttu&g_ep=EgoyMDI2MDUxNy4wIKXMDSoASAFQAw%3D%3D.

Google, 2026b. *Cyprus, 35°N 33°E*. Google Maps. Available at: https://www.google.com/maps/@35.0956738,33.3089435,184912m/data=!3m1!1e3?entry=ttu&g_ep=EgoyMDI2MDUxNy4wIKXMDSoASAFQAw%3D%3D.

Grahn, M., Malmgren, E., Korberg, A.D., Taljegard, M., Anderson, J.E., Brynolf, S., Wood, T. and Wallington, T.J., 2022. Review of electrofuel feasibility—cost and environmental impact. *Progress in Energy*, 4(3), p. 032010.

Huang, Y., Xu, D., Deng, S., and Lin, M., 2024. A hybrid electro-thermochemical device for methane production from the air. *Nature Communications*, 15(1), p. 8935.

International Energy Agency, 2026. *Cyprus*. Available at: https://www.iea.org/countries/cyprus.

International Organization for Standardization, 2017. *Solar energy — Solar thermal collectors — Test methods* (ISO Standard No. 9806:2017). Available at: https://www.iso.org/standard/67992.html.

Izam, N.S.M.N., Itam, Z., Sing, W.L. and Syamsir, A., 2022. Sustainable development perspectives of solar energy technologies with focus on solar Photovoltaic—A review. *Energies*, 15(8), p. 2790.

Jaaz, A.H., Hasan, H.A., Sopian, K., Kadhum, A.A.H., Gaaz, T.S. and Al-Amiery, A.A., 2017. Outdoor performance analysis of a photovoltaic thermal (PVT) collector with jet impingement and compound parabolic concentrator (CPC). *Materials*, 10(8), p. 888.

Kiss, A.A., Pragt, J.J., Vos, H.J., Bargeman, G. and De Groot, M.T., 2016. Novel efficient process for methanol synthesis by CO2 hydrogenation. *Chemical Engineering Journal*, 284, pp. 260-269.

Kramer, K.S., Mehnert, S., Munz, G., Helmling, S. and Lämmle, M., 2023. Photovoltaic thermal technology collectors, systems, and applications. *Energy Technology*, 11(12), p. 2300378.

Kumar, S.S. and Lim, H., 2022. An overview of water electrolysis technologies for green hydrogen production. *Energy Reports*, 8, pp. 13793-13813.

Lämmle, M., Oliva, A., Hermann, M., Kramer, K. and Kramer, W., 2017. PVT collector technologies in solar thermal systems: A systematic assessment of electrical and thermal yields with the novel characteristic temperature approach. *Solar Energy*, 155, pp. 867-879.

Lazoglou, G., Hadjinicolaou, P., Sofokleous, I., Bruggeman, A. and Zittis, G., 2024. Climate change and extremes in the Mediterranean island of Cyprus: from historical trends to future projections. *Environmental Research Communications*, 6(9), p. 095020.

Liu, J., Zhou, Y., Zhou, Z., Du, Y., Wang, C., Yang, X., Zhou, X., Shi, Y., Song, J. and Yan, J., 2024. Passive photovoltaic cooling: advances toward low-temperature operation. *Advanced Energy Materials*, 14(2), p. 2302662.

Malins, C., 2017. *What role is there for electrofuel technologies in European transport's low carbon future*. Cerulogy Report.

Masood, F., Nor, N.B.M., Nallagownden, P., Elamvazuthi, I., Saidur, R., Alam, M.A., Jamil, M. and Ali, M., 2022. A review of recent developments and applications of

compound parabolic concentrator-based hybrid solar photovoltaic/thermal collectors. *Sustainability*, 14(9), p. 5529.

Mazloomi, K., Sulaiman, N.B. and Moayedi, H., 2012. Electrical efficiency of electrolytic hydrogen production. *International Journal of Electrochemical Science*, 7(4), pp. 3314-3326.

Mehnert, S., Kramer, K., Geimer, K., Reinhardt, M., Fahr, S., Thoma, C., Kovac, P. and Ollas, P., 2017. *Guide to standard ISO 9806:2017: A resource for manufacturers, testing laboratories, certification bodies and regulatory agencies* (Version 1.0). Fraunhofer Institute for Solar Energy Systems; RISE Research Institutes of Sweden. Available at: https://www.researchgate.net/publication/320623512.

Neophytides, S.P., Eliades, M., Mavrovouniotis, M., Papoutsa, C., Papadavid, G. and Hadjimitsis, D.G., 2024. Improved water resources management for smart farming: a case study for Cyprus. *Scientific Reports*, 14(1), p. 31751.

Ridjan, I., 2015. *Integrated electrofuels and renewable energy systems*. Ph.D. thesis. Department of Development and Planning, Aalborg University, pp. 5-6.

Saldaña, J., Yurukcu, M., Boppana, N., Arbabi, S., Henry, J. and Ziyanak, S., 2025. Conventional and fossil fuels. In: *Energy transition in the oil and gas industry*. CRC Press, pp. 24-30.

Siecker, J., Kusakana, K. and Numbi, E.B., 2017. A review of solar photovoltaic systems cooling technologies. *Renewable and Sustainable Energy Reviews*, 79, pp. 192-203.

Skerlic, J., Nikolic, D., Cvetkovic, D. and Miškovic, A., 2018. Optimal Position of Solar Collectors: A Review. *Applied Engineering Letters*, 3, pp. 129–134.

Smit, B., 2016. Carbon capture and storage: introductory lecture. *Faraday Discussions*, 192, pp. 9-25.

Strobach, E., Faiman, D., Bader, S.J. and Hile, S.J., 2013. Effective incidence angles of sky-diffuse and ground-reflected irradiance for various incidence angle modifier types. *Solar Energy*, 89, pp. 81-88.

Vassiliko Cement Works Public Company Ltd., 2020. *Dispersion of share capital*. Available at: https://www.vassiliko.com/en/investor-relations/announcements/announcements-2020/dispersion-of-share-capital1039.

Xevgenos, D., Marcou, M., Louca, V., Avramidi, E., Ioannou, G., Argyrou, M., Stavrou, S., Mortou, M. and Küpper, F.C., 2021. Aspects of environmental impacts of seawater desalination: Cyprus as a case study. *Desalination and Water Treatment*, 211, pp. 15-30.

Zhang, H.L., Baeyens, J., Degrève, J. and Cáceres, G., 2013. Concentrated solar power plants: Review and design methodology. *Renewable and Sustainable Energy Reviews*, 22, pp. 466-481.